Elsevier Editorial System(tm) for Food and Chemical Toxicology
Manuscript Draft

Manuscript Number: FCT-D-11-01541R1

Title: Identification of novel mechanisms of silymarin on the carbon tetrachloride-induced liver fibrosis in mice by nuclear factor-κB bioluminescent imaging-guided transcriptomic analysis

Article Type: Full Length Article

Keywords: Liver fibrosis; Silymarin; Nuclear factor-κB; Bioluminescent imaging; DNA microarray; Cytochrome c oxidase

Corresponding Author: Prof. Tin-Yun Ho,

Corresponding Author's Institution: China Medical University

First Author: Chia-Cheng Li

Order of Authors: Chia-Cheng Li; Chien-Yun Hsiang; Shih-Lu Wu; Tin-Yun Ho

Abstract: In this study, we applied bioluminescent imaging-guided transcriptomic analysis to evaluate and identify the therapeutic potentials and novel mechanisms of silymarin on carbon tetrachloride (CCl_4)-induced liver fibrosis. Transgenic mice, carrying the luciferase genes driven by nuclear factor-κB (NF-κB), were given with CCl_4 and/or silymarin. In vivo NF-κB activity was evaluated by bioluminescent imaging, liver fibrosis was judged by Sirius red staining and immunohistochemistry, and gene expression profiles of silymarin-treated livers were analyzed by DNA microarray. CCl_4 enhanced the NF-κB-dependent hepatic luminescence and induced hepatic fibrosis, while silymarin reduced the CCl_4-induced hepatic luminescence and improved CCl_4-induced liver fibrosis. Microarray analysis showed that silymarin altered the transforming growth factor-β-mediated pathways, which play pivotal roles in the progression of liver fibrosis. Moreover, we newly identified that silymarin downregulated the expression levels of cytoskeleton organization genes and mitochondrion electron-transfer chain genes, such as cytochrome c oxidase Cox6a2, Cox7a1, and Cox8b genes. In conclusion, the correlation of NF-κB-dependent luminescence and liver fibrosis suggested the feasibility of NF-κB bioluminescent imaging for the evaluation of liver fibrosis progression and therapeutic potentials. Moreover, our findings suggested that silymarin might exhibit anti-fibrotic effects in vivo via altering the expression of genes involved in cytoskeleton organization and mitochondrion electron-transfer chain.

Response to Reviewers: Reviewer #2
1. Preparation of silymarin before oral administration should be stated in the MM section.
We have stated the preparation of silymarin in the "Materials and Methods" section (page 5, 2nd paragraph). The statement is described as follows.
Silymarin was purchased from Sigma (St. Louis, MO) and suspended in distilled water to a final concentration 20 mg/ml.

2. The author should describe the results shown by H&E staining in Figure 3. Where are the necrotic sites in Figure 3A?
We have stated the results shown by H&E staining in the "Results" section (page 10, last paragraph; page 11, 1st paragraph). We also have indicated the necrotic sites in Figure 3A. The statement is described as follows.

As shown in Fig. 3, no apparent pathological alternations were found in mock group. Sirius red-positive region in the mock group was appeared around the central vein but not in the hepatic parenchyma. CCl_4 damaged the lobular structure of liver, which was characterized by the infiltration of immune cells, hemorrhage, vacuolar degeneration, and necrosis of hepatocytes. Sirius red-stained areas were clearly appeared in the boundaries of liver lobules and the proportion of the hepatic fibrotic area was 3.86±0.54%. In contrast, silymarin improved the histological changes induced by CCl_4. The CCl_4-induced hemorrhage and necrosis in livers were ameliorated by silymarin. Moreover, Sirius red-stained areas in the silymarin group were reduced as compared with CCl_4 group, and the proportion of fibrotic areas (1.94±0.29%) was significantly decreased by silymarin. These data suggested that silymarin improved the CCl_4-induced liver fibrosis.

3. The histological analyses are not always clearly described: How many sections/fields were examined for each test?
For Sirius red staining quantification, 8 sections per group (10 fields per section) were examined and quantified. For immunohistochemical staining quantification, 8 sections per group (3 fields per section) were examined and quantified. We have supplemented these information in the "Figure Captions" section (pages 25-26).

4. For the PCR protocol, MIQE guidelines for publishing qPCR data have been issued see Clinical Chemistry 55:4 (2009) http://www.ncbi.nlm.nih.gov/pubmed/19246619 . According to these guidelines, some info is currently missing in the present manuscript such as:
(a)-was the efficiency of the PCR reaction measured?
(b)-Was a DNase treatment step added to remove chromosomal DNA, or any internal control added (eg. no reverse transcriptase control)?
(c)-Was the suitability of GAPDH as a reference gene tested?
(d) Which program was used to design the primers? Was primer specificity tested?
(a) We performed the serial dilution test to measure the efficiency of PCR. Briefly, a 4-log dilution range was generated using 10-fold serial dilutions of the DNA with four concentration points at 108, 107, 106, and 105 copies/μl. Quantitative PCR was performed as followed: 10 min at 95°C, and 40 cycles of 15 sec at 95°C, 1 min at 60°C using 2× Power SYBR Green PCR Master Mix (Applied Biosystems) and 200 nM of forward and reverse primers. Each assay was run on an Applied Biosystems 7300 Real-Time PCR system in triplicates. We have supplemented these information in the "Materials and Methods" section (page 8, lines -3∼-1).
(b) Total RNA was extracted from livers using the RNeasy Mini kit (Qiagen, Valencia, CA) and further treated with RNase-free DNase I (Qiagen, Valencia, CA) to remove contaminating DNA. We have supplemented these information in the "Materials and Methods" section (page 7, 2.5. Total RNA isolation).
(c) GAPDH gene is a well-known housekeeping gene and have been used as the reference gene for normalizing cellular proteins or genes. Previous study has shown that the levels of GAPDH mRNA and protein in livers are consistent in mice given with CCl_4 (Hellerbrand, C., Stefanovic, B., Giordano, F., Burchardt, E.R., and Brenner, D.A. 1999. The role of TGFβ1 in initiating hepatic stellate cell activation in vivo. J. Hepatol. 30: 77-87). Therefore, we used GAPDH gene as the reference gene in this study. We have supplemented these information in the "Materials and Methods" section (page 9, 1st paragraph).
(d) Primer sets used in this study were designed using Primer3 program (http://frodo.wi.mit.edu/primer3/). The specificities of primer sets were analyzed by nucleotide BLAST (http://blast.ncbi.nlm.nih.gov/Blast.cgi). Each primer set was able to amplify a target DNA fragment from the respective gene with specificity. We have supplemented these information in the "Materials and Methods" section (page 9, 1st paragraph).

5. The method of statistical analysis is not suitable since you are comparing more than two groups. If you are using parametric test, then the normality of the data has to be tested first followed by ANOVA and post hoc test such Duncan or LSD. Another way is to use non-parametric test such as Kruskall-

Wallis followed by Dunns post-hoc test. By performing this appropriate tes, this will definitely improved the quality of your data analysis.
The data have been analyzed by one-way ANOVA and post hoc LSD test using PASW Statistics (SPSS) version 12. A p value less than 0.05 was considered as statistically significant. We have supplemented these information in the "Materials and Methods" section (page 9, 2.8. Statistic analysis).

6. Could you explain why there was a basal NFKB activity at the lower part of the abdomen?
Transgenic mice used in this study contained luciferase genes driven by NF-κB-responsive elements. Therefore, the luciferase activity reflected the NF-κB trans-activity. When transgenic mice were injected intraperitoneally with D-luciferin and imaged, a diffuse luminescence was detected throughout the body and an intense signal was emitted at the lower part of the abdominal region (Fig. 1(A)). Ex vivo imaging showed that strong bioluminescent signals were detected in testis and prostate gland, which were located at the lower part of the abdominal region. Previous study has shown that NF-κB play an important role during the development of sperm cells (Lilienbaum, A., Sage, J., Mémet, S., Rassoulzadegan, M., Cuzin, F., and Israël, A. 2000. NF-κB is developmentally regulated during spermatogenesis in mice. Dev Dyn 219: 333-340). Therefore, these findings indicated that basal endogenous NF-κB activities in testis and prostate gland were strong, and the strong basal NF-κB activity at the lower part of the abdominal region was originated from these organs.

7. Could you explain the disparity of the % of fibrosis with the degree of fibrosis stained by Sirius Red? It is expected that the mice will show moderate degree of fibrosis at 8 weeks and the data presented is 12 weeks.
Figure 1 shows that administration of CCl4 significantly induced the NF-κB-dependent bioluminescent signal in the abdominal region, while oral administration of silymarin significantly suppressed the CCl4-induced luminescent intensity in the abdominal region and the suppression displayed a time-dependent manner. Therefore, we sacrificed mice on week 12 after CCl4 administration. H&E staining and Sirius red staining showed that pathological characteristics and the proportion of the hepatic fibrotic area were ameliorated and decreased by silymarin. These findings suggested that silymarin improved the CCl4-induced liver fibrosis on week 12 after CCl4 administration.

8. This study has shown that the TGF beta signaling pathway is involved. In order to validate the result stated in no. 7, I propose that alpha SMA should be evaluated at mRNA and protein expression level.
We evaluated the expression levels of TGF-β1, α-SMA, and NF-κB by quantifying TGF-β1, α-SMA, and NF-κB-positive regions in livers. Liver sections were immunostained with antibodies, and the proportions of TGF-β1, α-SMA, and NF-κB-positive areas were calculated as areas occupied with brown color/area of whole tissue. Data showed that the proportions of TGF-β1, α-SMA, and NF-κB-positive areas were increased in CCl4 group and decreased in silymarin group. These findings indicated that CCl4 induced the expression of TGF-β1, α-SMA, and NF-κB, while silymarin inhibited the CCl4-induced TGF-β1, α-SMA, and NF-κB expression. We have supplemented these information in the "Materials and Methods" section (page 7, 1st paragraph), "Results" section (page 11, 2nd paragraph), and "Figure 4".

Dear Dr. Delaney,

We would like to thank you for considering our article, as well as the referee for their critical reading and constructive remarks. We have revised our manuscript (FCT-D-11-01541) according to reviewers' comments. Our point-by-point reply to reviewers' comments is described in the "Response to Reviewers" section.

We thank you for your consideration of this matter and hope that our manuscript will be acceptable for publication in Food and Chemical Toxicology.

Yours sincerely,

Tin-Yun Ho

Reviewer #2

1. Preparation of silymarin before oral administration should be stated in the MM section.

   We have stated the preparation of silymarin in the "Materials and Methods" section (page 5, 2nd paragraph). The statement is described as follows.

   Silymarin was purchased from Sigma (St. Louis, MO) and suspended in distilled water to a final concentration 20 mg/ml.

2. The author should describe the results shown by H&E staining in Figure 3. Where are the necrotic sites in Figure 3A?

   We have stated the results shown by H&E staining in the "Results" section (page 10, last paragraph; page 11, 1st paragraph). We also have indicated the necrotic sites in Figure 3A. The statement is described as follows.

   As shown in Fig. 3, no apparent pathological alternations were found in mock group. Sirius red-positive region in the mock group was appeared around the central vein but not in the hepatic parenchyma. CCl_4 damaged the lobular structure of liver, which was characterized by the infiltration of immune cells, hemorrhage, vacuolar degeneration, and necrosis of hepatocytes. Sirius red-stained areas were clearly appeared in the boundaries of liver lobules and the proportion of the hepatic fibrotic area was 3.86±0.54%. In contrast, silymarin improved the histological changes induced by CCl_4. The CCl_4-induced hemorrhage and necrosis in livers were ameliorated by silymarin. Moreover, Sirius red-stained areas in the silymarin group were reduced as compared with CCl_4 group, and the proportion of fibrotic areas (1.94±0.29%) was significantly decreased by silymarin. These data suggested that silymarin improved the CCl_4-induced liver fibrosis.

3. The histological analyses are not always clearly described: How many sections/fields were examined for each test?

   For Sirius red staining quantification, 8 sections per group (10 fields per section) were examined and quantified. For immunohistochemical staining quantification, 8 sections per group (3 fields per section) were examined and quantified. We have supplemented

these information in the "Figure Captions" section (pages 25-26).

4. For the PCR protocol, MIQE guidelines for publishing qPCR data have been issued see Clinical Chemistry 55:4 (2009) http://www.ncbi.nlm.nih.gov/pubmed/19246619 . According to these guidelines, some info is currently missing in the present manuscript such as:

   (a)-was the efficiency of the PCR reaction measured?

   (b)-Was a DNase treatment step added to remove chromosomal DNA, or any internal control added (eg. no reverse transcriptase control)?

   (c)-Was the suitability of GAPDH as a reference gene tested?

   (d) Which program was used to design the primers? Was primer specificity tested?

(a) We performed the serial dilution test to measure the efficiency of PCR. Briefly, a 4-log dilution range was generated using 10-fold serial dilutions of the DNA with four concentration points at 10^8, 10^7, 10^6, and 10^5 copies/μl. Quantitative PCR was performed as followed: 10 min at 95℃, and 40 cycles of 15 sec at 95℃, 1 min at 60℃ using 2× Power SYBR Green PCR Master Mix (Applied Biosystems) and 200 nM of forward and reverse primers. Each assay was run on an Applied Biosystems 7300 Real-Time PCR system in triplicates. We have supplemented these information in the "Materials and Methods" section (page 8, lines -3~-1).

Results of serial dilution test are followed.

Gene	Slope	Intercept	R2
A	-3.62	39.45	0.99
B	-3.73	38.86	0.99

Gene A Gene B

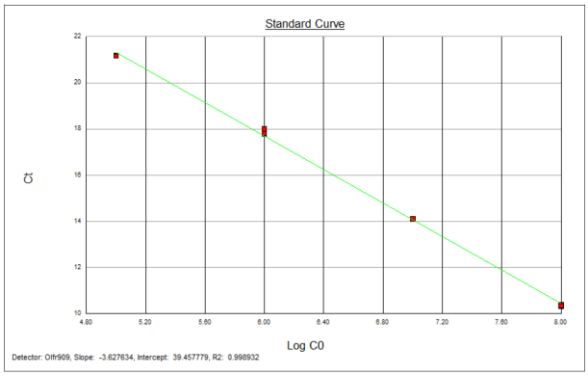

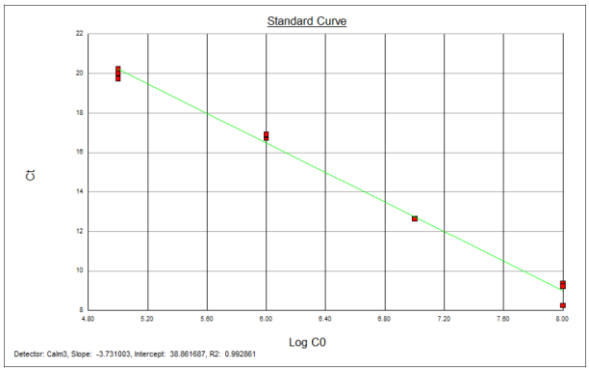

(b) Total RNA was extracted from livers using the RNeasy Mini kit (Qiagen, Valencia, CA) and further treated with RNase-free DNase I (Qiagen, Valencia, CA) to remove contaminating DNA. We have supplemented these information in the "Materials and Methods" section (page 7, 2.5. Total RNA isolation).

(c) GAPDH gene is a well-known housekeeping gene and have been used as the reference gene for normalizing cellular proteins or genes. Previous study has shown that the levels of GAPDH mRNA and protein in livers are consistent in mice given with CCl_4 (Hellerbrand, C., Stefanovic, B., Giordano, F., Burchardt, E.R., and Brenner, D.A. 1999. The role of TGFβ1 in initiating hepatic stellate cell activation in vivo. J. Hepatol. 30: 77-87). Therefore, we used GAPDH gene as the reference gene in this study. We have supplemented these information in the "Materials and Methods" section (page 9, 1st paragraph).

(d) Primer sets used in this study were designed using Primer3 program (http://frodo.wi.mit.edu/primer3/). The specificities of primer sets were analyzed by nucleotide BLAST (http://blast.ncbi.nlm.nih.gov/Blast.cgi). Each primer set was able to amplify a target DNA fragment from the respective gene with specificity. We have supplemented these information in the "Materials and Methods" section (page 9, 1st paragraph).

5. The method of statistical analysis is not suitable since you are comparing more than two groups. If you are using parametric test, then the normality of the data has to be tested first followed by ANOVA and post hoc test such Duncan or LSD. Another way is to use non-parametric test such as Kruskall-Wallis followed by Dunns post-hoc test.

By performing this appropriate tes, this will definitely improved the quality of your data analysis.

The data have been analyzed by one-way ANOVA and post hoc LSD test using PASW Statistics (SPSS) version 12. A *p* value less than 0.05 was considered as statistically significant. We have supplemented these information in the "Materials and Methods" section (page 9, *2.8.* Statistic analysis).

6. Could you explain why there was a basal NFKB activity at the lower part of the abdomen?

Transgenic mice used in this study contained luciferase genes driven by NF-κB-responsive elements. Therefore, the luciferase activity reflected the NF-κB trans-activity. When transgenic mice were injected intraperitoneally with D-luciferin and imaged, a diffuse luminescence was detected throughout the body and an intense signal was emitted at the lower part of the abdominal region (Fig. 1(A)). *Ex vivo* imaging showed that strong bioluminescent signals were detected in testis and prostate gland, which were located at the lower part of the abdominal region (see below). Previous study has shown that NF-κB play an important role during the development of sperm cells (Lilienbaum, A., Sage, J., Mémet, S., Rassoulzadegan, M., Cuzin, F., and Israël, A. 2000. NF-κB is developmentally regulated during spermatogenesis in mice. Dev Dyn 219: 333-340). Therefore, these findings indicated that basal endogenous NF-κB activities in testis and prostate gland were strong, and the strong basal NF-κB activity at the lower part of the abdominal region was originated from these organs.

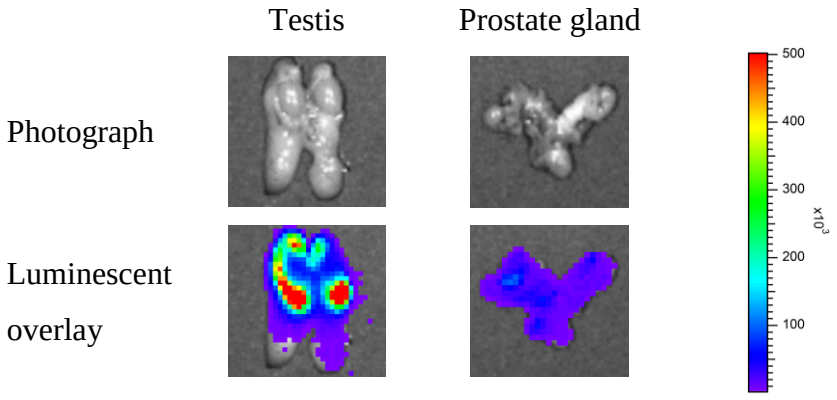

7. Could you explain the disparity of the % of fibrosis with the degree of fibrosis stained by Sirius Red? It is expected that the mice will show moderate degree of fibrosis at 8 weeks and the data presented is 12 weeks.

   Figure 1 shows that administration of CCl_4 significantly induced the NF-κB-dependent bioluminescent signal in the abdominal region, while oral administration of silymarin significantly suppressed the CCl_4-induced luminescent intensity in the abdominal region and the suppression displayed a time-dependent manner. Therefore, we sacrificed mice on week 12 after CCl_4 administration. H&E staining and Sirius red staining showed that pathological characteristics and the proportion of the hepatic fibrotic area were ameliorated and decreased by silymarin. These findings suggested that silymarin improved the CCl_4-induced liver fibrosis on week 12 after CCl_4 administration.

8. This study has shown that the TGF beta signaling pathway is involved. In order to validate the result stated in no. 7, I propose that alpha SMA should be evaluated at mRNA and protein expression level.

   We evaluated the expression levels of TGF-β1, α-SMA, and NF-κB by quantifying TGF-β1, α-SMA, and NF-κB-positive regions in livers. Liver sections were immunostained with antibodies, and the proportions of TGF-β1, α-SMA, and NF-κB-positive areas were calculated as areas occupied with brown color/area of whole tissue. Data showed that the proportions of TGF-β1, α-SMA, and NF-κB-positive areas were increased in CCl_4 group and decreased in silymarin group. These findings indicated that CCl_4 induced the expression of TGF-β1, α-SMA, and NF-κB, while silymarin inhibited the CCl_4-induced TGF-β1, α-SMA, and NF-κB expression. We have supplemented these information in the "Materials and Methods" section (page 7, 1st paragraph), "Results" section (page 11, 2nd paragraph), and "Figure 4".

ELSEVIER

Food and Chemical Toxicology

Conflict of Interest Policy

Supplement:
Article Title: Identification of novel mechanisms of silymarin on the carbon tetrachloride-induced liver fibrosis in mice by nuclear factor-κB bioluminescent imaging-guided transcriptomic analysis

Author name: Chia-Cheng Li, Chien-Yun Hsiang, Shih-Lu Wu, Tin-Yun Ho

Declarations

Food and Chemical Toxicology requires that all authors sign a declaration of conflicting interests. If you have nothing to declare in any of these categories then this should be stated.

Conflict of Interest

A conflicting interest exists when professional judgement concerning a primary interest (such as patient's welfare or the validity of research) may be influenced by a secondary interest (such as financial gain or personal rivalry). It may arise for the authors when they have financial interest that may influence their interpretation of their results or those of others. Examples of potential conflicts of interest include employment, consultancies, stock ownership, honoraria, paid expert testimony, patent applications/registrations, and grants or other funding.

Please state any competing interests

None

Funding Source

All sources of funding should also be acknowledged and you should declare any involvement of study sponsors in the study design; collection, analysis and interpretation of data; the writing of the manuscript; the decision to submit the manuscript for publication. If the study sponsors had no such involvement, this should be stated.

Please state any sources of funding for your research

None

Signature (a scanned signature is acceptable, but each author must sign)	**Print name**
Chia-Cheng Li	Chia-Cheng Li
Chienyun Hsiang	Chien-Yun Hsiang
Shih-Lu Wu	Shih-Lu Wu
Tin-Yun Ho	Tin-Yun Ho

Identification of novel mechanisms of silymarin on the carbon tetrachloride-induced liver fibrosis in mice by nuclear factor-κB bioluminescent imaging-guided transcriptomic analysis

Chia-Cheng Li[a], Chien-Yun Hsiang[b], Shih-Lu Wu[c], Tin-Yun Ho[a,d,*]

[a] Graduate Institute of Chinese Medicine, China Medical University, Taichung 40402, Taiwan

[b] Department of Microbiology, China Medical University, Taichung 40402, Taiwan

[c] Department of Biochemistry, China Medical University, Taichung 40402, Taiwan

[d] Department of Nuclear Medicine, China Medical University Hospital, Taichung 40447, Taiwan

[*]Corresponding author. Prof. Tin-Yun Ho, Graduate Institute of Chinese Medicine, China Medical University, 91 Hsueh-Shih Road, Taichung 40402, Taiwan. Tel: +886-4 22053366-3302. Fax: +886-4-22053764. E-mail: cyhsiang@mail.cmu.edu.tw

Abbreviations: CCl_4 , carbon tetrachloride; Cox, cytochrome *c* oxidase; GAPDH, glyceraldahyde-3-phosphate dehydrogenase; H&E, hematoxylin and eosin; NF-κB, nuclear factor-κB; α-SMA, α-smooth muscle actin; TGF-β, transforming growth factor-β

Highlights

> NF-κB bioluminescent imaging for evaluation of liver fibrosis progression.

> NF-κB bioluminescent imaging for evaluation of therapeutic potentials of silymarin.

>Silymarin exhibited anti-liver fibrotic activity in mice.

> Silymarin altered expressions of genes involved in cytoskeleton organization.

> Silymarin altered expressions of genes involved in mitochondrion respiratory chain.

Graphical Abstracts

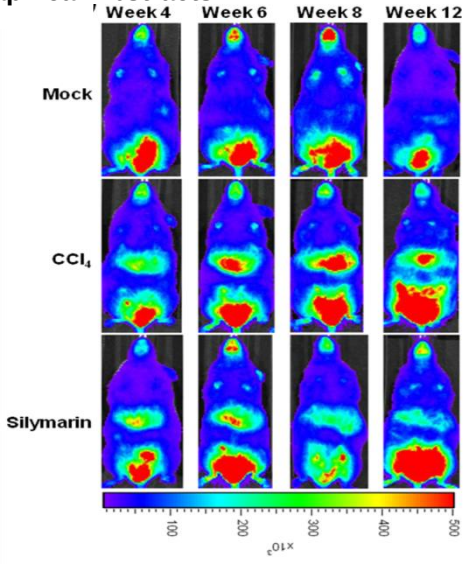

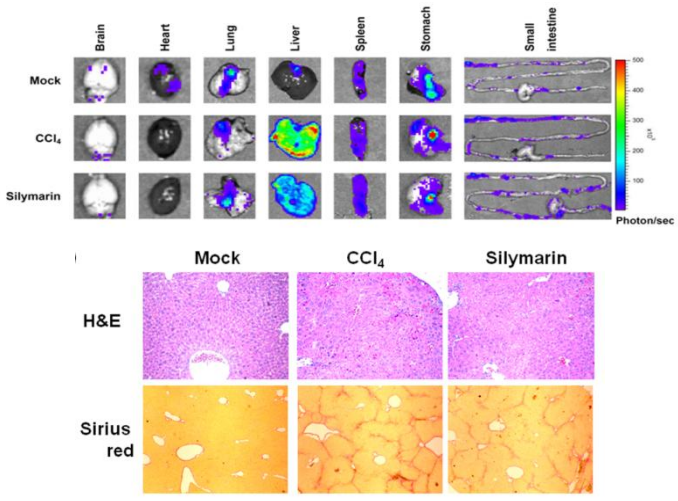

Table 2

Expression levels of silymarin-downregulated genes in CCl_4-treated liver.

Gene symbol	Description	Fold changes[a]
Acta1	Actin, alpha 1, skeletal muscle	-90.21±0.001
Myl1	Myosin, light polypeptide 1	-77.05±0.001
Tnni2	Troponin I, skeletal, fast 2	-49.39±0.001
Atp2a1	ATPase, Ca^{+2} transporting, cardiac muscle, fast twitch 1	-48.46±0.001
Mylpf	Myosin light chain, phosphorylatable, fast skeletal muscle	-41.90±0.001
Mb	Myoglobin	-35.39±0.002
Cox6a2	Cytochrome c oxidase, subunit VI a, polypeptide 2	-28.43±0.003
Cox8b	Cytochrome c oxidase, subunit VIII b	-18.60±0.004
Eno3	Enolase 3, beta muscle	-8.17±0.009
Tnnt1	Troponin T1, skeletal, slow	-7.60±0.011
Tnnc1	Troponin C, cardiac/slow skeletal	-7.56±0.010
Cox7a1	Cytochrome c oxidase, subunit VIIa 1	-6.67±0.015
Eef1a2	Eukaryotic translation elongation factor 1 alpha 2	-4.64±0.022
EG433229	Predicted gene, EG433229, transcript variant 7	-4.06±0.016

[a] Fold changes are mean ± standard error (n=3).

This work demonstrated the feasibility of NF-κB bioluminescent imaging for the evaluation of liver fibrosis progression and therapeutic potentials.

This work suggested that silymarin might exhibit anti-fibrotic effects *in vivo* via regulating TGF-β-mediated pathways and altering the expression of genes involved in cytoskeleton organization and mitochondrion electron-transfer chain.

Journal: Food and Chemical Toxicology
Manuscript title: Identification of novel mechanisms of silymarin on the carbon tetrachloride-induced liver fibrosis in mice by nuclear factor-κB bioluminescent imaging-guided transcriptomic analysis

Dear Editor,

Thank you for your useful comments and suggestions on the language and structure of our manuscript. We have modified the manuscript accordingly, and detailed corrections are listed below point by point:

1) Each bullet point provided in the Research Highlights should be within 85 characters (including spaces).

√ We have revised the bullet points provided in the Research Highlights. Each bullet point is within 85 characters (including spaces).

2) Please check the suggested reviewers instructions - there should be 4 reviewers of which 2 should be from a different country to the corresponding author. E-mail addresses containing hotmail, gmail, and yahoo accounts should not be used.

√ We have provided 4 suggested reviewers whose email addresses containing no hotmail and yahoo accounts.

The manuscript has been resubmitted to your journal. We look forward to your positive response.

Sincerely,

Tin-Yun Ho

Identification of novel mechanisms of silymarin on the carbon tetrachloride-induced liver fibrosis in mice by nuclear factor-κB bioluminescent imaging-guided transcriptomic analysis

Chia-Cheng Li[a], Chien-Yun Hsiang[b], Shih-Lu Wu[c], Tin-Yun Ho[a,d,*]

[a] Graduate Institute of Chinese Medicine, China Medical University, Taichung 40402, Taiwan

[b] Department of Microbiology, China Medical University, Taichung 40402, Taiwan

[c] Department of Biochemistry, China Medical University, Taichung 40402, Taiwan

[d] Department of Nuclear Medicine, China Medical University Hospital, Taichung 40447, Taiwan

[*]Corresponding author. Prof. Tin-Yun Ho, Graduate Institute of Chinese Medicine, China Medical University, 91 Hsueh-Shih Road, Taichung 40402, Taiwan. Tel: +886-4 22053366-3302. Fax: +886-4-22053764. E-mail: cyhsiang@mail.cmu.edu.tw

Abbreviations: CCl_4 , carbon tetrachloride; Cox, cytochrome *c* oxidase; GAPDH, glyceraldahyde-3-phosphate dehydrogenase; H&E, hematoxylin and eosin; NF-κB, nuclear factor-κB; α-SMA, α-smooth muscle actin; TGF-β, transforming growth factor-β

Abstract

In this study, we applied bioluminescent imaging-guided transcriptomic analysis to evaluate and identify the therapeutic potentials and novel mechanisms of silymarin on carbon tetrachloride (CCl_4)-induced liver fibrosis. Transgenic mice, carrying the luciferase genes driven by nuclear factor-κB (NF-κB), were given with CCl_4 and/or silymarin. *In vivo* NF-κB activity was evaluated by bioluminescent imaging, liver fibrosis was judged by Sirius red staining and immunohistochemistry, and gene expression profiles of silymarin-treated livers were analyzed by DNA microarray. CCl_4 enhanced the NF-κB-dependent hepatic luminescence and induced hepatic fibrosis, while silymarin reduced the CCl_4-induced hepatic luminescence and improved CCl_4-induced liver fibrosis. Microarray analysis showed that silymarin altered the transforming growth factor-β-mediated pathways, which play pivotal roles in the progression of liver fibrosis. Moreover, we newly identified that silymarin downregulated the expression levels of cytoskeleton organization genes and mitochondrion electron-transfer chain genes, such as cytochrome *c* oxidase Cox6a2, Cox7a1, and Cox8b genes. In conclusion, the correlation of NF-κB-dependent luminescence and liver fibrosis suggested the feasibility of NF-κB bioluminescent imaging for the evaluation of liver fibrosis progression and therapeutic potentials. Moreover, our findings suggested that silymarin might exhibit anti-fibrotic effects *in vivo* via altering the expression of genes involved in cytoskeleton organization and mitochondrion electron-transfer chain.

Keywords: Liver fibrosis, Silymarin, Nuclear factor-κB, Bioluminescent imaging, DNA microarray, Cytochrome *c* oxidase

1. Introduction

Liver fibrosis is a pathological sequel of chronic inflammatory liver injury caused by various etiologies, such as hepatitis virus infection, autoimmune injury, alcohol, and toxins/drugs. Following hepatic inflammation and damage, hepatic stellate cells change to myofibroblast-like cells and produce a large amount of extracellular matrix like type I collagen. The accumulation of collagen in the hepatic parenchyma further leads to the fibrosis of liver (Bataller and Brenner, 2005; Lotersztajn et al., 2005). Production of proinflammatory cytokines, such as interleukin-1β, tumor necrosis factor-α and interferon-γ, contribute to the progression of hepatic inflammation and sequential fibrosis (Luedde and Schwabe, 2011). The production of cytokines is further controlled by the transcription factor, nuclear factor-κB (NF-κB) (Baldwin, 1996). NF-κB is an inducible nuclear transcription factor that consists of heterodimers of RelA (p65), c-Rel, RelB, p50/NF-κB1, and p52/NF-κB2. NF-κB activity is activated by a large variety of stimuli, such as microbes, inflammatory cytokines, and physical and chemical stresses. When stimulated, NF-κB binds to the NF-κB-responsive element present in the promoters of inflammatory genes, resulting in the induction of gene expression and the inflammatory process. Accordingly, NF-κB is a critical molecule involved in the regulation of inflammatory cytokine production and inflammation (Bonizzi and Karin, 2004; Karin and Ben-Neriah, 2000; Siebenlist et al., 1994). Moreover, controlling NF-κB activation has become a pharmacological target, particularly in the chronic inflammatory disorders (Baeuerle and Baichwal, 1997).

Silymarin, a flavonoligan mixture of milk thistle (*Silybum marianum*), is an important herbal hepatoprotective drug (Abenavoli et al., 2010). Silymarin possesses a variety of pharmacological activities, such as anti-inflammatory, immunomodulatory,

anti-oxidant, and anti-viral activities (Polyak et al., 2007; Saller et al., 2001; Shaker et al., 2010). Silymarin exhibits hepatoprotective effects by altering cytoplasmic membrane architecture and, in turn, preventing the penetration of hepatotoxic substances, such as carbon tetrachloride (CCl_4), thioacetamide and D-galactosamine, into cells (Abenavoli et al., 2010; Basiglio et al., 2009). It also possesses the anti-fibrotic activity by retarding the activation of hepatic stellate cells (Chandan et al., 2008). Although the pharmacological mechanisms of silymarin have been reported, silymarin-altered hepatic gene expression profiles remained to be elucidated for the identification of novel targets and mechanisms for silymarin-mediated protection in the liver.

Bioluminescence imaging is a sensitive and noninvasive technique for real-time reporting and quantification of therapy efficacy in living animals (Hsu et al., 2010; Wu et al., 2009). This technique has been used for the assessment of host responses to biomaterials (Ho et al., 2007; Xiong et al., 2005)). It has also been applied for imaging disease progression and diagnosis (Dothager et al., 2009; Ottobrini et al., 2005). Microarray is a popular research and screening tool for differentially expressed genes. Microarray-based gene expression patterns have been used to predict the candidate biomarkers, predict the therapeutic efficacies of drugs, and recognize the toxic potential of drug candidate (Baur et al., 2006; Lamb et al., 2006; Suter et al., 2004). We have previously applied NF-κB bioluminescent imaging-guided transcriptomic analysis to assess the host responses to biomaterials and ionizing radiation *in vivo* (Ho et al., 2007; Hsiang et al., 2009). In this study, we applied NF-κB bioluminescent image to evaluate both the progression of CCl_4-induced liver injury and the therapeutic effects of silymarin. Microarray analysis was further applied to globally elucidate the gene expression profiles of silymarin and to find

novel mechanisms of silymarin on CCl_4-induced liver injury. Our data showed the feasibility of NF-κB-dependent bioluminescent image on the assessment of disease progression and therapeutic efficacies. Moreover, we newly identified that silymarin exhibited anti-fibrotic effects *in vivo* via regulating transforming growth factor-β (TGF-β)-mediated pathways and altering the expression of genes involved in cytoskeleton organization and mitochondrion electron-transfer chain.

2. Materials and methods

2.1. Induction of liver fibrosis and silymarin treatment

Mouse experiments were conducted under ethics approval from the China Medical University Animal Care and Use Committee. Transgenic mice, carrying the NF-κB-driven luciferase genes, were constructed previously (Ho et al., 2007). CCl_4-induced liver fibrosis was performed as described previously (Sakaida et al., 2004). Silymarin was purchased from Sigma (St. Louis, MO) and suspended in distilled water to a final concentration 20 mg/ml. A total of 24 transgenic mice was randomly divided into three groups of eight mice: (1) mock, mice were intraperitoneally administered with 0.5 ml/kg olive oil twice a week for 12 weeks, (2) CCl_4, mice were intraperitoneally administered with 0.5 ml/kg 10% CCl_4 in olive oil twice a week for 12 weeks, and (3) silymarin, mice were intraperitoneally administered with 0.5 ml/kg 10% CCl_4 in olive oil twice a week for 12 weeks, and silymarin was given orally at a dose of 200 mg/kg once a day from week 5 to 12 after CCl_4 administration.

2.2. In vivo and ex vivo imaging of luciferase activity

For *in vivo* imaging, mice were anesthetized with isoflurane and injected intraperitoneally with 150 mg luciferin/kg body weight. Five minutes later, mice were placed face up in the chamber and imaged for 1 min with the camera set at the highest sensitivity by IVIS Imaging System® 200 Series (Xenogen, Hopkinton, MA). For *ex vivo* imaging, mice were anesthetized and injected with luciferin intraperitoneally. Five minutes later, mice were sacrificed, and tissues were rapidly removed, placed in the IVIS system, and imaged with the same setting used for *in vivo* studies. Photons emitted from tissues were quantified using Living Image® software (Xenogen, Hopkinton, MA). Signal intensity was quantified as the sum of all detected photon counts from selected tissues and presented as photon/sec.

2.3. Quantitative analysis of liver fibrosis

For detecting hepatic fibrosis, liver sections were stained with 0.1% Sirius red (Sigma, St Louis, MO) in a saturated aqueous solution of picric acid (Panreac, Barcelona, Spain). One hour later, slides were rinsed in two changes of acidified water (0.5% glacial acetic acid in water), dehydrated in three changes of 100% ethanol, cleared in xylene, mounted in a resinous medium, and then observed under a light microscope. Sirius red-positive areas were measured using Image-Pro Plus (Media Cybernetics, Bethesda, MD). The proportions of hepatic fibrotic area (%) were calculated as areas occupied with red color/area of whole tissue.

2.4. Histological and immunohistochemical examination

Parafilm-embedded liver tissues were cut into 5-μm sections and stained with hematoxylin and eosin (H&E). For immunohistochemistry, sections were deparaffinized in xylene and rehydrated in graded alcohol. Endogenous peroxidase

was quenched with 3% hydrogen peroxide in methanol for 15 min and the nonspecific binding was blocked with 1% bovine serum albumin at room temperature for 1 h. Sections were incubated with antibodies against p65 (Chemicon, Temecula, CA), TGF-β1 (Santa Cruz, Santa Cruz, CA), or α-smooth muscle actin (α-SMA) (Santa Cruz, Santa Cruz, CA) at 1:50 dilution overnight at 4°C and then incubated with biotinylated secondary antibody (Zymed Laboratories, Carlsbad, CA) at room temperature for 20 min. Finally, slides were incubated with avidin-biotin complex reagent and stained with 3,3'-diaminobenzidine according to manufacturer's protocol (Histostain®-Plus kit, Zymed Laboratories, Carlsbad, CA). TGF-β1, α-SMA, and NF-κB-positive areas were measured using Image-Pro Plus (Media Cybernetics, Bethesda, MD) to quantify the expression levels of TGF-β1, α-SMA, and NF-κB. The proportions of TGF-β1, α-SMA, and NF-κB-positive areas were calculated as areas occupied with brown color/area of whole tissue.

2.5. Total RNA isolation

Total RNA was extracted from livers using the RNeasy Mini kit (Qiagen, Valencia, CA) and further treated with RNase-free DNase I (Qiagen, Valencia, CA) to remove contaminating DNA. Total RNA was quantified using the spectrophotometer (Beckman Coulter, Fullerton, CA), and samples with A260/A280 ratios greater than 1.8 were further evaluated using Agilent 2100 bioanalyzer (Agilent Technologies, Santa Clara, CA). The RNA sample with a RNA integrity number greater than 8.0 was accepted for microarray analysis

2.6. Microarray analysis

Microarray analysis was performed as described previously (Cheng et al., 2010).

Briefly, fluorescent RNA targets were prepared from 5 μg of total RNA using MessageAmp™ aRNA kit (Ambion, Austin, TX) and Cy5 dye (Amersham Pharmacia, Piscataway, NJ). Fluorescent targets were hybridized to the Mouse WG-6 Expression Bead Chip (Immunina, San Diego, CA) and scanned by an Axon 4000 scanner (Molecular Devices, Sunnyvale, CA). Number of replicates was three. The Cy5 fluorescent intensity of each spot was analyzed by genepix 4.1 software (Molecular Devices, Sunnyvale, CA). The signal intensity of each spot was corrected by subtracting background signals in the surrounding. We filtered out spots that signal-to-noise ratio was less than 0 or control probes. Spots that passed these criteria were normalized by the limma package of the R program using quantile normalization. Normalized data were tested for differential expression using Gene Expression Pattern Analysis Suite v3.1 (Montaner et al., 2006). Genes with fold changes ≥2.0 or ≤-2.0 were further selected and tested enriched pathways on WebGestalt web site (http://bioinfo.vanderbilt.edu/webgestalt/login.php) by hypergeometric test.

2.7. Quantitative real-time polymerase chain reaction (qPCR)

The expression levels of cytochrome *c* oxidase genes (Cox6a2, Cox7a1, and Cox8b) were validated by qPCR. RNA samples were reverse-transcribed for 2 h at 37°C with High Capacity cDNA Reverse Transcription kit (Applied Biosystems, Foster City, CA). qPCR was performed by using 1 μl of cDNA, 2× SYBR Green PCR Master Mix (Applied Biosystems, Foster City, CA), and 200 nM of forward and reverse primers. The reaction condition was followed: 10 min at 95°C, and 40 cycles of 15 sec at 95°C, 1 min at 60°C. Each assay was run on an Applied Biosystems 7300 Real-Time PCR system in triplicates. The efficiency of PCR was measured by the serial dilution test. A 4-log dilution range was generated using 10-fold serial dilutions of the DNA with

four concentration points at 10^8, 10^7, 10^6, and 10^5 copies/μl. Fold changes were calculated using the comparative C_T method. Primer sets used in this study were designed using Primer3 program (http://frodo.wi.mit.edu/primer3/). The specificities of primer sets were analyzed by nucleotide BLAST (http://blast.ncbi.nlm.nih.gov/Blast.cgi). Each primer set was able to amplify a target DNA fragment from the respective gene with specificity. The primer set for each gene is followed: Cox6a2 forward, 5'-CAGAGAAGGACAGTGCCATTC-3'; Cox6a2 reverse, 5'-GAAGAGCCAGCACAAAGGTC-3'; Cox7a1 forward, 5'-CAATGACCTCCCAGTACACTTG-3'; Cox7a1 reverse, 5'-CCAAGCAGTATAAGCAGTAGGC-3'; Cox8b forward, 5'-TCCCAAAGCCCATGTCTCTG-3'; Cox8b reverse, 5'-CATCCTGCTGGAACCATGAAG-3'; glyceraldahyde-3-phosphate dehydrogenase (GAPDH) forward, 5′-TCACCCACACTGTGCCCATCTATGA-3′; GAPDH reverse, 5′-GAGGAAGAGGATGCGGCAGTGG-3′. Previous study has shown that the levels of GAPDH mRNA and protein in livers are consistent in mice given with CCl_4 (Hellerbrand et al., 1999). Therefore, we used GAPDH gene as the reference gene in this study.

2.8. Statistic analysis

Data were presented as mean ± standard error. Data were analyzed by one-way ANOVA and post hoc LSD test using PASW Statistics (SPSS) version 12. A p value less than 0.05 was considered as statistically significant.

3. Results

3.1. Silymarin exhibited a steady decrease of CCl_4-induced NF-κB activity in the liver

Transgenic mice were given with CCl_4 and/or silymarin and imaged for the NF-κB-driven luminescence on week 4, 6, 8, and 12. As shown in Fig. 1, administration of CCl_4 significantly induced the NF-κB-dependent bioluminescent signal in the abdominal region as compared with mock group. *Ex vivo* imaging displayed that CCl_4 specifically induced the luminescence in the liver (Fig. 2). Oral administration of silymarin significantly suppressed the CCl_4-induced luminescent intensity in the abdominal region and the suppression displayed a time-dependent manner. *Ex vivo* imaging also displayed that silymarin specifically reduced CCl_4-induced NF-κB-driven bioluminescence in the liver. These findings suggested that CCl_4 induced NF-κB activation in the liver with specificity, while silymarin displayed a steady decrease of CCl_4-induced NF-κB activity in the liver.

3.2. The decrease of NF-κB activity by silymarin in the liver was correlated with the improvement of liver fibrosis

To evaluate the histological changes of liver and the degree of liver fibrosis, we stained the hepatic sections with H&E and Sirius red. Hepatic fibrosis is induced by the accumulation of collagen in the hepatic parenchyma (Bataller and Brenner, 2005). Sirius red is a strong anionic dye that has been used for the quantification of collagen in tissue sections for many years (Jimenez et al., 1985; Lopez-De Leon and Rojkind, 1985). Therefore, Sirius red-positive area can be a direct marker for the degree of liver fibrosis. As shown in Fig. 3, no apparent pathological alternations were found in mock group. Sirius red-positive region in the mock group was appeared around the central vein but not in the hepatic parenchyma. CCl_4 damaged the lobular structure of liver, which was characterized by the infiltration of immune cells, hemorrhage, vacuolar degeneration, and necrosis of hepatocytes. Sirius red-stained areas were clearly

appeared in the boundaries of liver lobules and the proportion of the hepatic fibrotic area was 3.86±0.54%. In contrast, silymarin improved the histological changes induced by CCl_4. The CCl_4-induced hemorrhage and necrosis in livers were ameliorated by silymarin. Moreover, Sirius red-stained areas in the silymarin group were reduced as compared with CCl_4 group, and the proportion of fibrotic areas (1.94±0.29%) was significantly decreased by silymarin. These data suggested that silymarin improved the CCl_4-induced liver fibrosis.

We further performed immunohistochemical staining to correlate the liver fibrosis with NF-κB activity. Liver sections were immunostained with α-SMA antibody to detect the presence of myofibroblasts that produce collagen (Wells, 2005). Sections were also immunostained with antibody against TGF-β1, a cytokine playing a pivotal role in the liver fibrosis (Lotersztajn et al., 2005). As shown in Fig. 4, there were many brown TGF-β1-positive cells and α-SMA-positive myofibroblasts in the CCl_4-treated liver. However, oral administration of silymarin decreased the number of brown cells in the liver. The proportions of TGF-β1, α-SMA, and NF-κB-positive areas were increased in CCl_4 group and decreased in silymarin group, suggesting that CCl_4 induced the expression of TGF-β1, α-SMA, and NF-κB, while silymarin inhibited the CCl_4-induced TGF-β1, α-SMA, and NF-κB expression. Moreover, these findings suggested that silymarin ameliorated CCl_4-induced liver fibrosis, which was coincident with aforementioned histological data. Immunostaining with antibody against p65 revealed that there were many brown p65-positive cells in the CCl_4-treated liver. However, silymarin decreased the number of p65-positive cells in the liver. These data suggested that silymarin might improve CCl_4-induced liver fibrosis via inhibition of NF-κB, TGF-β1, and α-SMA. Moreover, the correlation between NF-κB activity, liver fibrosis, and bioluminescent imaging suggested the

feasibility of NF-κB-dependent bioluminescent imaging for the evaluation of therapeutic efficacy of drugs for hepatic fibrosis.

3.3. Analysis of gene expression profile of silymarin in the CCl_4-treated liver

We further analyzed the gene expression profile of silymarin-treated liver by DNA microarray to identify the novel mechanisms of silymarin. In comparison with mock, 420 transcripts were upregulated and 439 transcripts were downregulated by 2-fold by CCl_4. In comparison with CCl_4, the expressions of 67 transcripts, including 2 upregulated and 65 downregulated transcripts, were altered with fold changes ≥ 2.0 or $\leq$-2.0 by silymarin. These genes were further selected for pathway classification. Table 1 shows that 34 pathways were significantly altered by silymarin ($p < 0.01$). The half of pathways was associated with metabolism, while others were related to regulation of cellular process and signal transduction. TGF-β-associated pathways, including TGF-β signaling pathway, TGF-β-induced apoptosis and TGF-β-mediated pathway, were significantly regulated by silymarin. Because TGF-β1 plays a pivotal role in the progression of liver fibrosis, alteration of TGF-β-related pathways might contribute to the improvement of CCl_4-induced liver fibrosis by silymarin. Silymarin downregulated the expression levels of 65 genes in the CCl_4-treated liver. The genes with fold changes $\leq$-4.0 are shown in Table 2. The half of silymarin-downregulated genes was associated with cytoskeleton organization and muscle contraction, while three genes, including Cox6a2, Cox7a2 and Cox8b genes, were related to mitochondrion electron-transport chain. These findings suggested that silymarin might improve the CCl_4-induced liver fibrosis via regulation the expression of genes involved in cytoskeleton organization and electron transport.

3.4. Verification of expression levels of novel silymarin-regulated genes by qPCR

Microarray data showed that the expression of mitochondrial respiratory chain-related genes, including Cox6a2, Cox7a1 and Cox8b genes, were downregulated by silymarin. We further applied qPCR to validate the transcriptional expression levels of these genes. As shown in Table 3, the expression levels of Cox6a2, Cox7a1, and Cox8b genes in CCl_4 group were 496.21, 21.36, and 240.38-fold higher, respectively, as compared with mock group. However, CCl_4-upregulated gene expression was downregulated by silymarin, and the expression levels of Cox6a2, Cox7a1, and Cox8b genes in silymarin group were 9.84, 0.72, and 0.7-fold, respectively, as compared with mock group. The consistent data from qPCR and microarray indicated that silymarin downregulated the CCl_4-induced expression of Cox6a2, Cox7a1, and Cox8b genes.

4. Discussion

In this study, we found that silymarin exhibited a steady decrease of CCl_4-induced NF-κB activity in the liver, and the decrease of NF-κB activity by silymarin in the liver was correlated with the improvement of liver fibrosis. During a steady decrease of CCl_4-induced NF-κB-dependent luminescence by silymarin, microarray analysis of liver showed that silymarin altered the TGF-β-mediated pathways. Moreover, we newly identified that novel target genes like Cox genes were downregulated by silymarin, which was evidenced by NF-κB bioluminescence imaging-guided transcriptomic analysis. Bioluminescence imaging is a sensitive and noninvasive technique for real-time reporting disease progression and quantifying therapy efficacies in living animals. This technique has been used for monitoring tumor cell

trafficking, tumor targeting, and host-biomaterial interaction (Contag and Bachmann, 2002; Ho et al., 2007; Ottobrini et al., 2005; Xiong et al., 2005). It has also been used to predict hepatic tumor burden in mice (Sarraf-Yazdi et al., 2004). In previous studies, we have constructed the transgenic mice carrying the NF-κB-driven luciferase gene and demonstrated the feasibility of NF-κB-dependent bioluminescent imaging for assessing the host-biomaterials interaction, elucidating the host response to ionizing radiation, evaluating the therapeutic effects of vanillin in inflammatory bowel diseases, and analyzing the anti-inflammatory effects of *Antrodia camphorata* (Chang et al., 2011; Ho et al., 2007; Hseu et al., 2010; Wu et al., 2009). In this study, we applied bioluminescent imaging to evaluate the progression of CCl_4-induced liver damages. Liver injury induced by CCl_4 is the best-characterized mechanism of xenobiotic-induced hepatotoxicity and a commonly used model for the screening of anti-hepatotoxic and/or hepatoprotective drugs (Weber et al., 2003). CCl_4 is metabolized by cytochrome p450 system and converted to trichloromethyl and trichloromethyl peroxy radicals. The free radicals of CCl_4 bind covalently to macromolecules and cause lipid peroxidation, which results in the fatty infiltration of hepatocytes and the sequential liver damage and fibrosis (Comporti et al., 2009). CCl_4 has been used extensively to induce liver injury in various animal models for decades. The experimentally induced cirrhotic response by CCl_4 in rats and mice are similar to liver cirrhosis in human (Weiler-Normann et al., 2007). Traditionally, liver injury and liver fibrosis induced by hepatotoxic substances can be evaluated by histological changes and concentrations of alanine aminotransferase, aspartate aminotransferase, alkaline phosphatase, and γ-glutamyl transpeptidase in sera (Nanji et al., 2001; Sun et al., 2010; Tacke et al., 2005)). Because the sustained hepatic inflammation induced by various etiologies leads to liver fibrosis, and NF-κB plays a critical role in regulating

inflammatory responses (Luedde and Schwabe, 2011), we tried to apply NF-κB transgenic mice to report the liver fibrosis induced by CCl_4. CCl_4 induced the NF-κB-dependent luminescence in the liver with specificity and the NF-κB activation was correlated with liver fibrosis, judged by Sirius red staining and immunohistochemical analysis. These findings indicated the feasibility of NF-κB bioluminescent imaging on the reporting of liver fibrosis induced by CCl_4.

Silymarin is a well-known hepatoprotective agent for the treatment of liver diseases (Abenavoli et al., 2010). It possesses antioxidative, antilipid peroxidative, antifibrotic, membrane stabilizing, immunomodulatory, and liver regenerating activities (Polyak et al., 2007; Saller et al., 2001; Shaker et al., 2010). Silymarin offers a good protection in various models of experimental liver diseases. It has also been applied clinically for alcoholic liver diseases, liver cirrhosis, Amanita mushroom poisoning, and drug-induced liver diseases (Pradhan and Girish, 2006). In this study, bioluminescent imaging showed that oral administration of silymarin reduced the CCl_4-induced NF-κB-dependent luminescent intensity in the liver with specificity. The correlation of the decreased NF-κB activity and the improved liver fibrosis by silymarin, suggesting the feasibility of NF-κB-dependent bioluminescent imaging for the evaluation of therapeutic effect of silymarin *in vivo*.

NF-κB bioluminescent imaging-guided transcriptomic analysis was further applied for the evaluation of novel targets and mechanisms of silymarin-mediated protection in the liver. Previous studies indicated that the anti-fibrotic and anti-inflammatory effects of silymarin are associated with TGF-β1 pathway (Ai et al., 2010). Silymarin suppresses the expression of profibrotic procollagen-α and TIMP-1 via downregulation of TGF-β1 mRNA in rats with biliary fibrosis (Jia et al., 2001). Moreover, genes associated with oxidative stress, cell cycle, cytoskeletal network,

cell-cell adhesion, extracellular matrix, inflammation, and apoptosis are altered by silymarin in pyrogallol-exposed liver (Upadhyay et al., 2010). In this study, microarray data showed that silymarin altered the TGF-β1-associated pathways, including TGF-β signaling pathway, TGF-β-induced apoptosis and TGF-β-mediated pathway, in CCl_4-induced liver fibrosis, which were in agreement with previous reports. Furthermore, we newly identified that silymarin downregulated the expression levels of cytoskeleton organization genes and mitochondrion electron-transfer chain genes. It has been known that CCl_4 treatment induces the reorganization of cytoskeleton and, in turn, induces the differentiation of hepatic stellate cells into myofibroblast-like cells ((De Minicis et al., 2007). Silymarin downregulated the expression of cytoskeleton component genes, suggesting that silymarin might suppress the transformation of hepatic stellate cells via inhibiting cytoskeleton reorganization and thus ameliorate the fibrosis of liver. Progression of CCl_4-induced liver fibrosis is associated with free radicals production that results in the significant alternations in functional state of mitochondrial respiratory chain (Tanaka et al., 1987). The electron transporters are combined in four complex: NADH reductase, succinate reductase, cytochrome *c* reductase, and Cox (Boyer, 1997). Cox plays a crucial role in oxidative metabolism, acting as the terminal component of the mitochondrial electron-transport chain in which electrons are passed from cytochrome *c* to molecular oxygen (Boyer, 1997). Previous studies showed that CCl_4 treatment decreases the activity of NADH reductase and increases the activity of Cox in rats with CCl_4-induced liver fibrosis (Krahenbuhl and Reichen, 1992; Shiryaeva et al., 2008; Tanaka et al., 1987). Our data also showed that the expression levels of Cox genes were elevated by CCl_4. The decrease and damage of NADH reductase results in electron leakage to $\cdot O_2^-$ oxygen and superoxide anion production, which lead to the

increased oxygen consumption by the respiratory chain of pathologic mitochondria. Subsequently, the elevated activity of Cox by CCl_4 promotes the transfer of electrons to molecular oxygen and drive the ATP production of the mitochondria (Shiryaeva et al., 2008). In contrast, previous study indicated that silymarin inhibits the oxygen consumption in mitochondria isolated from rats and increases the iron-reduced NADH reductase activity to the basal level (Chavez and Bravo, 1988; Pietrangelo et al., 2002). Moreover, our data showed that silymarin reduced the CCl_4-induced expression levels of Cox genes to the basal levels as compared to mock. These findings suggested that silymarin might counteract the mitochondrion electron-transfer chain alteration by CCl_4, which might be associated with the improvement of CCl_4-induced liver fibrosis by silymarin.

5. Conclusions

In conclusion, we applied for the first time the *in vivo* NF-κB bioluminescent imaging and microarray analysis for the evaluation and identification of the therapeutic potentials and novel mechanisms of silymarin in CCl_4-induced liver fibrosis. The correlation of NF-κB bioluminescence and liver fibrosis suggested the feasibility of NF-κB bioluminescent imaging on the evaluation of therapeutic potentials of drugs for the treatment of liver fibrosis. Moreover, we newly identified that silymarin exhibited anti-fibrotic effects *in vivo* via regulating TGF-β-mediated pathways and altering the expression of genes involved in cytoskeleton organization and mitochondrion electron-transfer chain.

Conflict of Interest

The authors declare that there are no conflicts of interest.

Acknowledgments

This work was supported by grants from National Science Council, Committee on Chinese Medicine and Pharmacy at Department of Health (CCMP100-RD-048), and China Medical University (CMU100-S-16, CMU100-S-34, and CMU100-TS-14).

References

Abenavoli, L., Capasso, R., Milic, N., Capasso, F., 2010. Milk thistle in liver diseases: past, present, future. Phytother Res 24, 1423-1432.

Ai, W., Zhang, Y., Tang, Q.Z., Yan, L., Bian, Z.Y., Liu, C., Huang, H., Bai, X., Yin, L., Li, H., 2010. Silibinin attenuates cardiac hypertrophy and fibrosis through blocking EGFR-dependent signaling. J Cell Biochem 110, 1111-1122.

Baeuerle, P.A., Baichwal, V.R., 1997. NF-κB as a frequent target for immunosuppressive and anti-inflammatory molecules. Adv Immunol. 65, 111-137.

Baldwin, A.S., Jr., 1996. The NF-κB and IκB proteins: new discoveries and insights. Annu Rev Immunol 14, 649-683.

Basiglio, C.L., Sanchez Pozzi, E.J., Mottino, A.D., Roma, M.G., 2009. Differential effects of silymarin and its active component silibinin on plasma membrane stability and hepatocellular lysis. Chem Biol Interact 179, 297-303.

Bataller, R., Brenner, D.A., 2005. Liver fibrosis. J Clin Invest 115, 209-218.

Baur, J.A., Pearson, K.J., Price, N.L., Jamieson, H.A., Lerin, C., Kalra, A., Prabhu, V.V., Allard, J.S., Lopez-Lluch, G., Lewis, K., Pistell, P.J., Poosala, S., Becker, K.G., Boss, O., Gwinn, D., Wang, M., Ramaswamy, S., Fishbein, K.W., Spencer, R.G., Lakatta, E.G., Le Couteur, D., Shaw, R.J., Navas, P., Puigserver, P., Ingram, D.K., de Cabo, R., Sinclair, D.A., 2006. Resveratrol improves health and survival of mice on a high-calorie diet. Nature 444, 337-342.

Bonizzi, G., Karin, M., 2004. The two NF-κB activation pathways and their role in innate and adaptive immunity. Trends Immunol 25, 280-288.

Boyer, P.D., 1997. The ATP synthase--a splendid molecular machine. Annual review of biochemistry 66, 717-749.

Chandan, B.K., Saxena, A.K., Shukla, S., Sharma, N., Gupta, D.K., Singh, K., Suri, J., Bhadauria, M., Qazi, G.N., 2008. Hepatoprotective activity of Woodfordia fruticosa Kurz flowers against carbon tetrachloride induced hepatotoxicity. J Ethnopharmacol 119, 218-224.

Chang, C.T., Lin, H., Ho, T.Y., Li, C.C., Lo, H.Y., Wu, S.L., Huang, Y.F., Liang, J.A., Hsiang, C.Y., 2011. Comprehensive assessment of host responses to ionizing radiation by nuclear factor-κB bioluminescence imaging-guided transcriptomic analysis. PLoS ONE, in press.

Chavez, E., Bravo, C., 1988. Silymarin-induced mitochondrial Ca2+ release. Life Sci 43, 975-981.

Cheng, H.M., Li, C.C., Chen, C.Y., Lo, H.Y., Cheng, W.Y., Lee, C.H., Yang, S.Z., Wu, S.L., Hsiang, C.Y., Ho, T.Y., 2010. Application of bioactivity database of Chinese herbal medicine on the therapeutic prediction, drug development, and safety evaluation. J Ethnopharmacol 132, 429-437.

Comporti, M., Arezzini, B., Signorini, C., Vecchio, D., Gardi, C., 2009. Oxidative stress, isoprostanes and hepatic fibrosis. Histol Histopathol 24, 893-900.

Contag, C.H., Bachmann, M.H., 2002. Advances in *in vivo* bioluminescence imaging of gene expression. Annu Rev Biomed Eng 4, 235-260.

De Minicis, S., Seki, E., Uchinami, H., Kluwe, J., Zhang, Y., Brenner, D.A., Schwabe, R.F., 2007. Gene expression profiles during hepatic stellate cell activation in culture and *in vivo*. Gastroenterology 132, 1937-1946.

Dothager, R.S., Flentie, K., Moss, B., Pan, M.H., Kesarwala, A., Piwnica-Worms, D., 2009. Advances in bioluminescence imaging of live animal models. Curr Opin Biotechnol 20, 45-53.

Hellerbrand, C., Stefanovic, B., Giordano, F., Burchardt, E.R., Brenner, D.A. 1999.

The role of TGFβ1 in initiating hepatic stellate cell activation *in vivo*. J Hepatol 30, 77-87.

Ho, T.Y., Chen, Y.S., Hsiang, C.Y., 2007. Noninvasive nuclear factor-κB bioluminescence imaging for the assessment of host-biomaterial interaction in transgenic mice. Biomaterials 28, 4370-4377.

Hseu, Y.C., Huang, H.C., Hsiang, C.Y., 2010. *Antrodia camphorata* suppresses lipopolysaccharide-induced nuclear factor-κB activation in transgenic mice evaluated by bioluminescence imaging. Food Chem Toxicol 48, 2319-2325.

Hsiang, C.Y., Chen, Y.S., Ho, T.Y., 2009. Nuclear factor-κB bioluminescence imaging-guided transcriptomic analysis for the assessment of host-biomaterial interaction *in vivo*. Biomaterials 30, 3042-3049.

Jia, J.D., Bauer, M., Cho, J.J., Ruehl, M., Milani, S., Boigk, G., Riecken, E.O., Schuppan, D., 2001. Antifibrotic effect of silymarin in rat secondary biliary fibrosis is mediated by downregulation of procollagen alpha1(I) and TIMP-1. J Hepatol 35, 392-398.

Jimenez, W., Pares, A., Caballeria, J., Heredia, D., Bruguera, M., Torres, M., Rojkind, M., Rodes, J., 1985. Measurement of fibrosis in needle liver biopsies: evaluation of a colorimetric method. Hepatology 5, 815-818.

Karin, M., Ben-Neriah, Y., 2000. Phosphorylation meets ubiquitination: the control of NF-κB activity. Annu Rev Immunol 18, 621-663.

Krahenbuhl, S., Reichen, J., 1992. Adaptation of mitochondrial metabolism in liver cirrhosis. Different strategies to maintain a vital function. Scand J Gastroenterol Suppl 193, 90-96.

Lamb, J., Crawford, E.D., Peck, D., Modell, J.W., Blat, I.C., Wrobel, M.J., Lerner, J., Brunet, J.P., Subramanian, A., Ross, K.N., Reich, M., Hieronymus, H., Wei, G.,

Armstrong, S.A., Haggarty, S.J., Clemons, P.A., Wei, R., Carr, S.A., Lander, E.S., Golub, T.R., 2006. The Connectivity Map: using gene-expression signatures to connect small molecules, genes, and disease. Science 313, 1929-1935.

Lopez-De Leon, A., Rojkind, M., 1985. A simple micromethod for collagen and total protein determination in formalin-fixed paraffin-embedded sections. J Histochem Cytochem 33, 737-743.

Lotersztajn, S., Julien, B., Teixeira-Clerc, F., Grenard, P., Mallat, A., 2005. Hepatic fibrosis: molecular mechanisms and drug targets. Annu Rev Pharmacol Toxicol 45, 605-628.

Luedde, T., Schwabe, R.F., 2011. NF-κB in the liver--linking injury, fibrosis and hepatocellular carcinoma. Nat Rev Gastroenterol Hepatol 8, 108-118.

Nanji, A.A., Jokelainen, K., Tipoe, G.L., Rahemtulla, A., Dannenberg, A.J., 2001. Dietary saturated fatty acids reverse inflammatory and fibrotic changes in rat liver despite continued ethanol administration. J Pharmacol Exp Ther 299, 638-644.

Ottobrini, L., Lucignani, G., Clerici, M., Rescigno, M., 2005. Assessing cell trafficking by noninvasive imaging techniques: applications in experimental tumor immunology. Q J Nucl Med Mol Imaging 49, 361-366.

Pietrangelo, A., Montosi, G., Garuti, C., Contri, M., Giovannini, F., Ceccarelli, D., Masini, A., 2002. Iron-induced oxidant stress in nonparenchymal liver cells: mitochondrial derangement and fibrosis in acutely iron-dosed gerbils and its prevention by silybin. J Bioenerg Biomembr 34, 67-79.

Polyak, S.J., Morishima, C., Shuhart, M.C., Wang, C.C., Liu, Y., Lee, D.Y., 2007. Inhibition of T-cell inflammatory cytokines, hepatocyte NF-κB signaling, and HCV infection by standardized Silymarin. Gastroenterology 132, 1925-1936.

Pradhan, S.C., Girish, C., 2006. Hepatoprotective herbal drug, silymarin from

experimental pharmacology to clinical medicine. Indian J Med Res 124, 491-504.

Sakaida, I., Terai, S., Yamamoto, N., Aoyama, K., Ishikawa, T., Nishina, H., Okita, K., 2004. Transplantation of bone marrow cells reduces CCl_4-induced liver fibrosis in mice. Hepatology 40, 1304-1311.

Saller, R., Meier, R., Brignoli, R., 2001. The use of silymarin in the treatment of liver diseases. Drugs 61, 2035-2063.

Sarraf-Yazdi, S., Mi, J., Dewhirst, M.W., Clary, B.M., 2004. Use of *in vivo* bioluminescence imaging to predict hepatic tumor burden in mice. J Surg Res 120, 249-255.

Shaker, E., Mahmoud, H., Mnaa, S., Silymarin, the antioxidant component and *Silybum marianum* extracts prevent liver damage. Food Chem Toxicol 48, 803-806.

Shiryaeva, A., Baidyuk, E., Arkadieva, A., Okovityy, S., Morozov, V., Sakuta, G., 2008. Hepatocyte mitochondrion electron-transport chain alterations in CCl_4 and alcohol induced hepatitis in rats and their correction with simvastatin. J Bioenerg Biomembr 40, 27-34.

Siebenlist, U., Franzoso, G., Brown, K., 1994. Structure, regulation and function of NF-κB. Annu Rev Cell Biol 10, 405-455.

Sun, H., Che, Q.M., Zhao, X., Pu, X.P., 2010. Antifibrotic effects of chronic baicalein administration in a CCl_4 liver fibrosis model in rats. Eur J Pharmacol 631, 53-60.

Suter, L., Babiss, L.E., Wheeldon, E.B., 2004. Toxicogenomics in predictive toxicology in drug development. Chem Biol 11, 161-171.

Tacke, F., Wustefeld, T., Horn, R., Luedde, T., Srinivas Rao, A., Manns, M.P., Trautwein, C., Brabant, G., 2005. High adiponectin in chronic liver disease and cholestasis suggests biliary route of adiponectin excretion *in vivo*. J Hepatol 42,

666-673.

Tanaka, A., Morimoto, T., Wakashiro, S., Ikai, I., Ozawa, K., Orii, Y., 1987. Kinetic alterations of cytochrome *c* oxidase in carbon tetrachloride induced cirrhotic rat liver. Life Sci 41, 741-748.

Upadhyay, G., Tiwari, M.N., Prakash, O., Jyoti, A., Shanker, R., Singh, M.P., 2010. Involvement of multiple molecular events in pyrogallol-induced hepatotoxicity and silymarin-mediated protection: evidence from gene expression profiles. Food Chem Toxicol 48, 1660-1670.

Weiler-Normann, C., Herkel, J., Lohse, A.W., 2007. Mouse models of liver fibrosis. Z Gastroenterol 45, 43-50.

Wells, R.G., 2005. The role of matrix stiffness in hepatic stellate cell activation and liver fibrosis. J Clin Gastroenterol 39, S158-161.

Wu, S.L., Chen, J.C., Li, C.C., Lo, H.Y., Ho, T.Y., Hsiang, C.Y., 2009. Vanillin improves and prevents trinitrobenzene sulfonic acid-induced colitis in mice. J Pharmacol Exp Ther 330, 370-376.

Xiong, Y.Q., Willard, J., Kadurugamuwa, J.L., Yu, J., Francis, K.P., Bayer, A.S., 2005. Real-time *in vivo* bioluminescent imaging for evaluating the efficacy of antibiotics in a rat Staphylococcus aureus endocarditis model. Antimicrob Agents Chemother 49, 380-387.

Figure captions

Fig. 1. NF-κB-dependent bioluminescence in living mice. Transgenic mice were administered with CCl_4 and/or silymarin, and imaged at indicated periods. (A) *In vivo* imaging. The color overlay on the image represents the photon/sec emitted from the animal, as indicated by the color scales. Photos are representative images (n=8). (B) Quantification of photon emission from whole animal. Values are mean ± standard error (n=8). ###p<0.001, compared with mock. *p<0.05, **p<0.01, compared with CCl_4.

Fig. 2. NF-κB-dependent bioluminescence in individual organs. Transgenic mice were administered with CCl_4 and/or silymarin. Twelve weeks later, mice were sacrificed and organs were subjected to image. (A) *Ex vivo* imaging. The color overlay on the image represents the photon/sec emitted from the organ, as indicated by the color scales. Photos are representative images (n=8). (B) Quantification of photon emission from organs. Values are mean ± standard error (n=8). ###p<0.001, compared with mock. ***p<0.001, compared with CCl_4.

Fig. 3. Histological examination of liver by H&E and Sirius red staining. (A) Histological examination. Transgenic mice were administered with CCl_4 and/or silymarin. Twelve weeks later, mice were sacrificed, livers were excised, and sections were stained with H&E (100× magnification) or Sirius red (40× magnification). Photos are representative images (n=8). (B) Quantification of liver fibrosis by Sirius red stain. Results are expressed as fibrotic area (%), which was calculated as areas occupied with red color/area of whole tissue. Values are mean ± standard error (8 sections/group and 10 fields/section). ###p<0.001, compared with

mock. ***$p<0.001$, compared with CCl_4.

Fig. 4. Immunohistochemical examination of liver. Transgenic mice were administered with CCl_4 and/or silymarin. Twelve weeks later, mice were sacrificed, livers were excised, and sections were immunostained with antibodies against TGF-β1, α-SMA, and p65 (100× magnification). Quantification of TGF-β1, α-SMA, and p65-positive areas (%) was shown at the bottom. Values are mean ± standard error (8 sections/group and 3 fields/section). Photos are representative images (n=8).

Table1

Pathway analysis of silymarin-altered genes with fold changes ≥2.0 or ≤–2.0.

Pathway	*p* value[a]
Regulation of cellular process/ cell cycle and death	
TGF-β signaling pathway	2.75×10^{-7}
p53-mediated pathway	0.00171
Tight junction	0.00014
TGF-β-induced apoptosis	0.00261
Adherens junction	0.00494
TGF-β-mediated pathway	0.00976
Metabolism	
Urea cycle and metabolism of amino groups	2.49×10^{-5}
Citrate cycle	2.45×10^{-6}
Arginine and proline metabolism	0.00016
Galactose metabolism	0.00034
Biosynthesis of steroids	0.00049
Glycine, serine and threonine metabolism	0.00070
Glycolysis / Gluconeogenesis	0.00100
Butanoate metabolism	0.00098
Folate biosynthesis	0.00218
Pyruvate metabolism	0.00223
Fatty acid metabolism	0.00273
Bile acid biosynthesis	0.00273
Alanine and aspartate metabolism	0.00442
Glutathione metabolism	0.00544
Starch and sucrose metabolism	0.00601
Glycosaminoglycan degradation	0.00799
Glutamate metabolism	0.00921
Signal tansduction	
Adipocytokine signaling pathway	8.26×10^{-5}
IL6 signaling pathway	0.00016
PPAR signaling pathway	0.00039
Insulin signaling pathway	0.00047
Vitamin D3 signaling pathway	0.00067
RANKL signaling pathway	0.00548
TNF signaling pathway	0.00629
IGF signaling pathway	0.00655
Chemokine signaling pathway	0.00709
EGF signaling pathway	0.00770
PTH/PTHrP signaling pathway	0.00840

[a] *p* value was calculated on WebGestalt web site by hypergeometric test.

Table 2

Expression levels of silymarin-downregulated genes in CCl_4-treated liver.

Gene symbol	Description	Fold changes[a]
Acta1	Actin, alpha 1, skeletal muscle	-90.21±0.001
Myl1	Myosin, light polypeptide 1	-77.05±0.001
Tnni2	Troponin I, skeletal, fast 2	-49.39±0.001
Atp2a1	ATPase, Ca^{+2} transporting, cardiac muscle, fast twitch 1	-48.46±0.001
Mylpf	Myosin light chain, phosphorylatable, fast skeletal muscle	-41.90±0.001
Mb	Myoglobin	-35.39±0.002
Cox6a2	Cytochrome c oxidase, subunit VI a, polypeptide 2	-28.43±0.003
Cox8b	Cytochrome c oxidase, subunit VIII b	-18.60±0.004
Eno3	Enolase 3, beta muscle	-8.17±0.009
Tnnt1	Troponin T1, skeletal, slow	-7.60±0.011
Tnnc1	Troponin C, cardiac/slow skeletal	-7.56±0.010
Cox7a1	Cytochrome c oxidase, subunit VIIa 1	-6.67±0.015
Eef1a2	Eukaryotic translation elongation factor 1 alpha 2	-4.64±0.022
EG433229	Predicted gene, EG433229, transcript variant 7	-4.06±0.016

[a] Fold changes are mean ± standard error (n=3).

Table 3

Expression levels of Cox6a2, Cox7a1, and Cox8b genes by qPCR.

Sample	Average C_T of target	Average C_T of GAPDH	ΔC_T[a]	$\Delta\Delta C_T$[b]	Relative to mock
Cox6a2					
Mock	35.82 ± 0.40	19.71 ± 0.03	16.11 ± 0.40	0.00 ± 0.40	1.00
CCl_4	25.80 ± 0.05	18.64 ± 0.05	7.16 ± 0.07	-8.96 ± 0.07	496.21
Silymarin	31.17 ± 0.09	18.36 ± 0.01	12.81 ± 0.09	-3.30 ± 0.09	9.84
Cox7a1					
Mock	29.98 ± 0.10	19.71 ± 0.03	10.27 ± 0.11	0.00 ± 0.11	1.00
CCl_4	24.49 ± 0.04	18.64 ± 0.05	5.85 ± 0.07	-4.42 ± 0.07	21.36
Silymarin	29.10 ±0 .11	18.36 ± 0.01	10.74 ± 0.11	0.47 ± 0.11	0.72
Cox8b					
Mock	32.81 ± 0.11	19.71 ± 0.03	13.09 ± 0.12	0.00 ± 0.12	1.00
CCl_4	23.83 ± 0.05	18.64 ± 0.05	5.18 ± 0.07	-7.91 ± 0.07	240.38
Silymarin	31.97 ± 0.29	18.36 ± 0.01	13.61 ± 0.29	0.52 ± 0.29	0.70

[a] The ΔC_T value is determined by subtracting the average GAPDH C_T value from the average target gene C_T value. The standard deviation of the difference is calculated from the standard deviations of the target gene and GAPDH.

[b] The calculation of $\Delta\Delta C_T$ involves subtraction by the ΔC_T calibrator value. This is a subtraction of an arbitrary constant, so the standard

deviation of$\Delta\Delta C_T$ is the same as the standard deviation of ΔC_T value.

Identification of novel mechanisms of silymarin on the carbon tetrachloride-induced liver fibrosis in mice by nuclear factor-κB bioluminescent imaging-guided transcriptomic analysis

Chia-Cheng Li[a], Chien-Yun Hsiang[b], Shih-Lu Wu[c], Tin-Yun Ho[a,d,*]

[a] Graduate Institute of Chinese Medicine, China Medical University, Taichung 40402, Taiwan

[b] Department of Microbiology, China Medical University, Taichung 40402, Taiwan

[c] Department of Biochemistry, China Medical University, Taichung 40402, Taiwan

[d] Department of Nuclear Medicine, China Medical University Hospital, Taichung 40447, Taiwan

[*]Corresponding author. Prof. Tin-Yun Ho, Graduate Institute of Chinese Medicine, China Medical University, 91 Hsueh-Shih Road, Taichung 40402, Taiwan. Tel: +886-4 22053366-3302. Fax: +886-4-22053764. E-mail: cyhsiang@mail.cmu.edu.tw

Abbreviations: CCl_4 , carbon tetrachloride; Cox, cytochrome *c* oxidase; GAPDH, glyceraldahyde-3-phosphate dehydrogenase; H&E, hematoxylin and eosin; NF-κB, nuclear factor-κB; α-SMA, α-smooth muscle actin; TGF-β, transforming growth factor-β

Abstract

In this study, we applied bioluminescent imaging-guided transcriptomic analysis to evaluate and identify the therapeutic potentials and novel mechanisms of silymarin on carbon tetrachloride (CCl_4)-induced liver fibrosis. Transgenic mice, carrying the luciferase genes driven by nuclear factor-κB (NF-κB), were given with CCl_4 and/or silymarin. *In vivo* NF-κB activity was evaluated by bioluminescent imaging, liver fibrosis was judged by Sirius red staining and immunohistochemistry, and gene expression profiles of silymarin-treated livers were analyzed by DNA microarray. CCl_4 enhanced the NF-κB-dependent hepatic luminescence and induced hepatic fibrosis, while silymarin reduced the CCl_4-induced hepatic luminescence and improved CCl_4-induced liver fibrosis. Microarray analysis showed that silymarin altered the transforming growth factor-β-mediated pathways, which play pivotal roles in the progression of liver fibrosis. Moreover, we newly identified that silymarin downregulated the expression levels of cytoskeleton organization genes and mitochondrion electron-transfer chain genes, such as cytochrome *c* oxidase Cox6a2, Cox7a1, and Cox8b genes. In conclusion, the correlation of NF-κB-dependent luminescence and liver fibrosis suggested the feasibility of NF-κB bioluminescent imaging for the evaluation of liver fibrosis progression and therapeutic potentials. Moreover, our findings suggested that silymarin might exhibit anti-fibrotic effects *in vivo* via altering the expression of genes involved in cytoskeleton organization and mitochondrion electron-transfer chain.

Keywords: Liver fibrosis, Silymarin, Nuclear factor-κB, Bioluminescent imaging, DNA microarray, Cytochrome *c* oxidase

1. Introduction

Liver fibrosis is a pathological sequel of chronic inflammatory liver injury caused by various etiologies, such as hepatitis virus infection, autoimmune injury, alcohol, and toxins/drugs. Following hepatic inflammation and damage, hepatic stellate cells change to myofibroblast-like cells and produce a large amount of extracellular matrix like type I collagen. The accumulation of collagen in the hepatic parenchyma further leads to the fibrosis of liver (Bataller and Brenner, 2005; Lotersztajn et al., 2005). Production of proinflammatory cytokines, such as interleukin-1β, tumor necrosis factor-α and interferon-γ, contribute to the progression of hepatic inflammation and sequential fibrosis (Luedde and Schwabe, 2011). The production of cytokines is further controlled by the transcription factor, nuclear factor-κB (NF-κB) (Baldwin, 1996). NF-κB is an inducible nuclear transcription factor that consists of heterodimers of RelA (p65), c-Rel, RelB, p50/NF-κB1, and p52/NF-κB2. NF-κB activity is activated by a large variety of stimuli, such as microbes, inflammatory cytokines, and physical and chemical stresses. When stimulated, NF-κB binds to the NF-κB-responsive element present in the promoters of inflammatory genes, resulting in the induction of gene expression and the inflammatory process. Accordingly, NF-κB is a critical molecule involved in the regulation of inflammatory cytokine production and inflammation (Bonizzi and Karin, 2004; Karin and Ben-Neriah, 2000; Siebenlist et al., 1994). Moreover, controlling NF-κB activation has become a pharmacological target, particularly in the chronic inflammatory disorders (Baeuerle and Baichwal, 1997).

Silymarin, a flavonoligan mixture of milk thistle (*Silybum marianum*), is an important herbal hepatoprotective drug (Abenavoli et al., 2010). Silymarin possesses a variety of pharmacological activities, such as anti-inflammatory, immunomodulatory,

anti-oxidant, and anti-viral activities (Polyak et al., 2007; Saller et al., 2001; Shaker et al., 2010). Silymarin exhibits hepatoprotective effects by altering cytoplasmic membrane architecture and, in turn, preventing the penetration of hepatotoxic substances, such as carbon tetrachloride (CCl_4), thioacetamide and D-galactosamine, into cells (Abenavoli et al., 2010; Basiglio et al., 2009). It also possesses the anti-fibrotic activity by retarding the activation of hepatic stellate cells (Chandan et al., 2008). Although the pharmacological mechanisms of silymarin have been reported, silymarin-altered hepatic gene expression profiles remained to be elucidated for the identification of novel targets and mechanisms for silymarin-mediated protection in the liver.

Bioluminescence imaging is a sensitive and noninvasive technique for real-time reporting and quantification of therapy efficacy in living animals (Hsu et al., 2010; Wu et al., 2009). This technique has been used for the assessment of host responses to biomaterials (Ho et al., 2007; Xiong et al., 2005)). It has also been applied for imaging disease progression and diagnosis (Dothager et al., 2009; Ottobrini et al., 2005). Microarray is a popular research and screening tool for differentially expressed genes. Microarray-based gene expression patterns have been used to predict the candidate biomarkers, predict the therapeutic efficacies of drugs, and recognize the toxic potential of drug candidate (Baur et al., 2006; Lamb et al., 2006; Suter et al., 2004). We have previously applied NF-κB bioluminescent imaging-guided transcriptomic analysis to assess the host responses to biomaterials and ionizing radiation *in vivo* (Ho et al., 2007; Hsiang et al., 2009). In this study, we applied NF-κB bioluminescent image to evaluate both the progression of CCl_4-induced liver injury and the therapeutic effects of silymarin. Microarray analysis was further applied to globally elucidate the gene expression profiles of silymarin and to find

novel mechanisms of silymarin on CCl_4-induced liver injury. Our data showed the feasibility of NF-κB-dependent bioluminescent image on the assessment of disease progression and therapeutic efficacies. Moreover, we newly identified that silymarin exhibited anti-fibrotic effects *in vivo* via regulating transforming growth factor-β (TGF-β)-mediated pathways and altering the expression of genes involved in cytoskeleton organization and mitochondrion electron-transfer chain.

2. Materials and methods

2.1. Induction of liver fibrosis and silymarin treatment

Mouse experiments were conducted under ethics approval from the China Medical University Animal Care and Use Committee. Transgenic mice, carrying the NF-κB-driven luciferase genes, were constructed previously (Ho et al., 2007). CCl_4-induced liver fibrosis was performed as described previously (Sakaida et al., 2004). Silymarin was purchased from Sigma (St. Louis, MO) and suspended in distilled water to a final concentration 20 mg/ml. A total of 24 transgenic mice was randomly divided into three groups of eight mice: (1) mock, mice were intraperitoneally administered with 0.5 ml/kg olive oil twice a week for 12 weeks, (2) CCl_4, mice were intraperitoneally administered with 0.5 ml/kg 10% CCl_4 in olive oil twice a week for 12 weeks, and (3) silymarin, mice were intraperitoneally administered with 0.5 ml/kg 10% CCl_4 in olive oil twice a week for 12 weeks, and silymarin was given orally at a dose of 200 mg/kg once a day from week 5 to 12 after CCl_4 administration.

2.2. In vivo and ex vivo imaging of luciferase activity

For *in vivo* imaging, mice were anesthetized with isoflurane and injected intraperitoneally with 150 mg luciferin/kg body weight. Five minutes later, mice were placed face up in the chamber and imaged for 1 min with the camera set at the highest sensitivity by IVIS Imaging System® 200 Series (Xenogen, Hopkinton, MA). For *ex vivo* imaging, mice were anesthetized and injected with luciferin intraperitoneally. Five minutes later, mice were sacrificed, and tissues were rapidly removed, placed in the IVIS system, and imaged with the same setting used for *in vivo* studies. Photons emitted from tissues were quantified using Living Image® software (Xenogen, Hopkinton, MA). Signal intensity was quantified as the sum of all detected photon counts from selected tissues and presented as photon/sec.

2.3. Quantitative analysis of liver fibrosis

For detecting hepatic fibrosis, liver sections were stained with 0.1% Sirius red (Sigma, St Louis, MO) in a saturated aqueous solution of picric acid (Panreac, Barcelona, Spain). One hour later, slides were rinsed in two changes of acidified water (0.5% glacial acetic acid in water), dehydrated in three changes of 100% ethanol, cleared in xylene, mounted in a resinous medium, and then observed under a light microscope. Sirius red-positive areas were measured using Image-Pro Plus (Media Cybernetics, Bethesda, MD). The proportions of hepatic fibrotic area (%) were calculated as areas occupied with red color/area of whole tissue.

2.4. Histological and immunohistochemical examination

Parafilm-embedded liver tissues were cut into 5-μm sections and stained with hematoxylin and eosin (H&E). For immunohistochemistry, sections were deparaffinized in xylene and rehydrated in graded alcohol. Endogenous peroxidase

was quenched with 3% hydrogen peroxide in methanol for 15 min and the nonspecific binding was blocked with 1% bovine serum albumin at room temperature for 1 h. Sections were incubated with antibodies against p65 (Chemicon, Temecula, CA), TGF-β1 (Santa Cruz, Santa Cruz, CA), or α-smooth muscle actin (α-SMA) (Santa Cruz, Santa Cruz, CA) at 1:50 dilution overnight at 4°C and then incubated with biotinylated secondary antibody (Zymed Laboratories, Carlsbad, CA) at room temperature for 20 min. Finally, slides were incubated with avidin-biotin complex reagent and stained with 3,3'-diaminobenzidine according to manufacturer's protocol (Histostain®-Plus kit, Zymed Laboratories, Carlsbad, CA). TGF-β1, α-SMA, and NF-κB-positive areas were measured using Image-Pro Plus (Media Cybernetics, Bethesda, MD) to quantify the expression levels of TGF-β1, α-SMA, and NF-κB. The proportions of TGF-β1, α-SMA, and NF-κB-positive areas were calculated as areas occupied with brown color/area of whole tissue.

2.5. Total RNA isolation

Total RNA was extracted from livers using the RNeasy Mini kit (Qiagen, Valencia, CA) and further treated with RNase-free DNase I (Qiagen, Valencia, CA) to remove contaminating DNA. Total RNA was quantified using the spectrophotometer (Beckman Coulter, Fullerton, CA), and samples with A260/A280 ratios greater than 1.8 were further evaluated using Agilent 2100 bioanalyzer (Agilent Technologies, Santa Clara, CA). The RNA sample with a RNA integrity number greater than 8.0 was accepted for microarray analysis

2.6. Microarray analysis

Microarray analysis was performed as described previously (Cheng et al., 2010).

Briefly, fluorescent RNA targets were prepared from 5 μg of total RNA using MessageAmp™ aRNA kit (Ambion, Austin, TX) and Cy5 dye (Amersham Pharmacia, Piscataway, NJ). Fluorescent targets were hybridized to the Mouse WG-6 Expression Bead Chip (Immunina, San Diego, CA) and scanned by an Axon 4000 scanner (Molecular Devices, Sunnyvale, CA). Number of replicates was three. The Cy5 fluorescent intensity of each spot was analyzed by genepix 4.1 software (Molecular Devices, Sunnyvale, CA). The signal intensity of each spot was corrected by subtracting background signals in the surrounding. We filtered out spots that signal-to-noise ratio was less than 0 or control probes. Spots that passed these criteria were normalized by the limma package of the R program using quantile normalization. Normalized data were tested for differential expression using Gene Expression Pattern Analysis Suite v3.1 (Montaner et al., 2006). Genes with fold changes ≥2.0 or ≤-2.0 were further selected and tested enriched pathways on WebGestalt web site (http://bioinfo.vanderbilt.edu/webgestalt/login.php) by hypergeometric test.

2.7. Quantitative real-time polymerase chain reaction (qPCR)

The expression levels of cytochrome *c* oxidase genes (Cox6a2, Cox7a1, and Cox8b) were validated by qPCR. RNA samples were reverse-transcribed for 2 h at 37°C with High Capacity cDNA Reverse Transcription kit (Applied Biosystems, Foster City, CA). qPCR was performed by using 1 μl of cDNA, 2× SYBR Green PCR Master Mix (Applied Biosystems, Foster City, CA), and 200 nM of forward and reverse primers. The reaction condition was followed: 10 min at 95°C, and 40 cycles of 15 sec at 95°C, 1 min at 60°C. Each assay was run on an Applied Biosystems 7300 Real-Time PCR system in triplicates. The efficiency of PCR was measured by the serial dilution test. A 4-log dilution range was generated using 10-fold serial dilutions of the DNA with

four concentration points at 10^8, 10^7, 10^6, and 10^5 copies/μl. Fold changes were calculated using the comparative C_T method. Primer sets used in this study were designed using Primer3 program (http://frodo.wi.mit.edu/primer3/). The specificities of primer sets were analyzed by nucleotide BLAST (http://blast.ncbi.nlm.nih.gov/Blast.cgi). Each primer set was able to amplify a target DNA fragment from the respective gene with specificity. The primer set for each gene is followed: Cox6a2 forward, 5'-CAGAGAAGGACAGTGCCATTC-3'; Cox6a2 reverse, 5'-GAAGAGCCAGCACAAAGGTC-3'; Cox7a1 forward, 5'-CAATGACCTCCCAGTACACTTG-3'; Cox7a1 reverse, 5'-CCAAGCAGTATAAGCAGTAGGC-3'; Cox8b forward, 5'-TCCCAAAGCCCATGTCTCTG-3'; Cox8b reverse, 5'-CATCCTGCTGGAACCATGAAG-3'; glyceraldahyde-3-phosphate dehydrogenase (GAPDH) forward, 5′-TCACCCACACTGTGCCCATCTATGA-3′; GAPDH reverse, 5′-GAGGAAGAGGATGCGGCAGTGG-3′. Previous study has shown that the levels of GAPDH mRNA and protein in livers are consistent in mice given with CCl_4 (Hellerbrand et al., 1999). Therefore, we used GAPDH gene as the reference gene in this study.

2.8. Statistic analysis

Data were presented as mean ± standard error. Data were analyzed by one-way ANOVA and post hoc LSD test using PASW Statistics (SPSS) version 12. A *p* value less than 0.05 was considered as statistically significant.

3. Results

3.1. Silymarin exhibited a steady decrease of CCl_4-induced NF-κB activity in the liver

Transgenic mice were given with CCl_4 and/or silymarin and imaged for the NF-κB-driven luminescence on week 4, 6, 8, and 12. As shown in Fig. 1, administration of CCl_4 significantly induced the NF-κB-dependent bioluminescent signal in the abdominal region as compared with mock group. *Ex vivo* imaging displayed that CCl_4 specifically induced the luminescence in the liver (Fig. 2). Oral administration of silymarin significantly suppressed the CCl_4-induced luminescent intensity in the abdominal region and the suppression displayed a time-dependent manner. *Ex vivo* imaging also displayed that silymarin specifically reduced CCl_4-induced NF-κB-driven bioluminescence in the liver. These findings suggested that CCl_4 induced NF-κB activation in the liver with specificity, while silymarin displayed a steady decrease of CCl_4-induced NF-κB activity in the liver.

3.2. The decrease of NF-κB activity by silymarin in the liver was correlated with the improvement of liver fibrosis

To evaluate the histological changes of liver and the degree of liver fibrosis, we stained the hepatic sections with H&E and Sirius red. Hepatic fibrosis is induced by the accumulation of collagen in the hepatic parenchyma (Bataller and Brenner, 2005). Sirius red is a strong anionic dye that has been used for the quantification of collagen in tissue sections for many years (Jimenez et al., 1985; Lopez-De Leon and Rojkind, 1985). Therefore, Sirius red-positive area can be a direct marker for the degree of liver fibrosis. As shown in Fig. 3, no apparent pathological alternations were found in mock group. Sirius red-positive region in the mock group was appeared around the central vein but not in the hepatic parenchyma. CCl_4 damaged the lobular structure of liver, which was characterized by the infiltration of immune cells, hemorrhage, vacuolar degeneration, and necrosis of hepatocytes. Sirius red-stained areas were clearly

appeared in the boundaries of liver lobules and the proportion of the hepatic fibrotic area was 3.86±0.54%. In contrast, silymarin improved the histological changes induced by CCl_4. The CCl_4-induced hemorrhage and necrosis in livers were ameliorated by silymarin. Moreover, Sirius red-stained areas in the silymarin group were reduced as compared with CCl_4 group, and the proportion of fibrotic areas (1.94±0.29%) was significantly decreased by silymarin. These data suggested that silymarin improved the CCl_4-induced liver fibrosis.

We further performed immunohistochemical staining to correlate the liver fibrosis with NF-κB activity. Liver sections were immunostained with α-SMA antibody to detect the presence of myofibroblasts that produce collagen (Wells, 2005). Sections were also immunostained with antibody against TGF-β1, a cytokine playing a pivotal role in the liver fibrosis (Lotersztajn et al., 2005). As shown in Fig. 4, there were many brown TGF-β1-positive cells and α-SMA-positive myofibroblasts in the CCl_4-treated liver. However, oral administration of silymarin decreased the number of brown cells in the liver. The proportions of TGF-β1, α-SMA, and NF-κB-positive areas were increased in CCl_4 group and decreased in silymarin group, suggesting that CCl_4 induced the expression of TGF-β1, α-SMA, and NF-κB, while silymarin inhibited the CCl_4-induced TGF-β1, α-SMA, and NF-κB expression. Moreover, these findings suggested that silymarin ameliorated CCl_4-induced liver fibrosis, which was coincident with aforementioned histological data. Immunostaining with antibody against p65 revealed that there were many brown p65-positive cells in the CCl_4-treated liver. However, silymarin decreased the number of p65-positive cells in the liver. These data suggested that silymarin might improve CCl_4-induced liver fibrosis via inhibition of NF-κB, TGF-β1, and α-SMA. Moreover, the correlation between NF-κB activity, liver fibrosis, and bioluminescent imaging suggested the

feasibility of NF-κB-dependent bioluminescent imaging for the evaluation of therapeutic efficacy of drugs for hepatic fibrosis.

3.3. Analysis of gene expression profile of silymarin in the CCl_4-treated liver

We further analyzed the gene expression profile of silymarin-treated liver by DNA microarray to identify the novel mechanisms of silymarin. In comparison with mock, 420 transcripts were upregulated and 439 transcripts were downregulated by 2-fold by CCl_4. In comparison with CCl_4, the expressions of 67 transcripts, including 2 upregulated and 65 downregulated transcripts, were altered with fold changes ≥ 2.0 or $\leq$-2.0 by silymarin. These genes were further selected for pathway classification. Table 1 shows that 34 pathways were significantly altered by silymarin ($p < 0.01$). The half of pathways was associated with metabolism, while others were related to regulation of cellular process and signal transduction. TGF-β-associated pathways, including TGF-β signaling pathway, TGF-β-induced apoptosis and TGF-β-mediated pathway, were significantly regulated by silymarin. Because TGF-β1 plays a pivotal role in the progression of liver fibrosis, alteration of TGF-β-related pathways might contribute to the improvement of CCl_4-induced liver fibrosis by silymarin. Silymarin downregulated the expression levels of 65 genes in the CCl_4-treated liver. The genes with fold changes $\leq$-4.0 are shown in Table 2. The half of silymarin-downregulated genes was associated with cytoskeleton organization and muscle contraction, while three genes, including Cox6a2, Cox7a2 and Cox8b genes, were related to mitochondrion electron-transport chain. These findings suggested that silymarin might improve the CCl_4-induced liver fibrosis via regulation the expression of genes involved in cytoskeleton organization and electron transport.

3.4. Verification of expression levels of novel silymarin-regulated genes by qPCR

Microarray data showed that the expression of mitochondrial respiratory chain-related genes, including Cox6a2, Cox7a1 and Cox8b genes, were downregulated by silymarin. We further applied qPCR to validate the transcriptional expression levels of these genes. As shown in Table 3, the expression levels of Cox6a2, Cox7a1, and Cox8b genes in CCl_4 group were 496.21, 21.36, and 240.38-fold higher, respectively, as compared with mock group. However, CCl_4-upregulated gene expression was downregulated by silymarin, and the expression levels of Cox6a2, Cox7a1, and Cox8b genes in silymarin group were 9.84, 0.72, and 0.7-fold, respectively, as compared with mock group. The consistent data from qPCR and microarray indicated that silymarin downregulated the CCl_4-induced expression of Cox6a2, Cox7a1, and Cox8b genes.

4. Discussion

In this study, we found that silymarin exhibited a steady decrease of CCl_4-induced NF-κB activity in the liver, and the decrease of NF-κB activity by silymarin in the liver was correlated with the improvement of liver fibrosis. During a steady decrease of CCl_4-induced NF-κB-dependent luminescence by silymarin, microarray analysis of liver showed that silymarin altered the TGF-β-mediated pathways. Moreover, we newly identified that novel target genes like Cox genes were downregulated by silymarin, which was evidenced by NF-κB bioluminescence imaging-guided transcriptomic analysis. Bioluminescence imaging is a sensitive and noninvasive technique for real-time reporting disease progression and quantifying therapy efficacies in living animals. This technique has been used for monitoring tumor cell

trafficking, tumor targeting, and host-biomaterial interaction (Contag and Bachmann, 2002; Ho et al., 2007; Ottobrini et al., 2005; Xiong et al., 2005). It has also been used to predict hepatic tumor burden in mice (Sarraf-Yazdi et al., 2004). In previous studies, we have constructed the transgenic mice carrying the NF-κB-driven luciferase gene and demonstrated the feasibility of NF-κB-dependent bioluminescent imaging for assessing the host-biomaterials interaction, elucidating the host response to ionizing radiation, evaluating the therapeutic effects of vanillin in inflammatory bowel diseases, and analyzing the anti-inflammatory effects of *Antrodia camphorata* (Chang et al., 2011; Ho et al., 2007; Hseu et al., 2010; Wu et al., 2009). In this study, we applied bioluminescent imaging to evaluate the progression of CCl_4-induced liver damages. Liver injury induced by CCl_4 is the best-characterized mechanism of xenobiotic-induced hepatotoxicity and a commonly used model for the screening of anti-hepatotoxic and/or hepatoprotective drugs (Weber et al., 2003). CCl_4 is metabolized by cytochrome p450 system and converted to trichloromethyl and trichloromethyl peroxy radicals. The free radicals of CCl_4 bind covalently to macromolecules and cause lipid peroxidation, which results in the fatty infiltration of hepatocytes and the sequential liver damage and fibrosis (Comporti et al., 2009). CCl_4 has been used extensively to induce liver injury in various animal models for decades. The experimentally induced cirrhotic response by CCl_4 in rats and mice are similar to liver cirrhosis in human (Weiler-Normann et al., 2007). Traditionally, liver injury and liver fibrosis induced by hepatotoxic substances can be evaluated by histological changes and concentrations of alanine aminotransferase, aspartate aminotransferase, alkaline phosphatase, and γ-glutamyl transpeptidase in sera (Nanji et al., 2001; Sun et al., 2010; Tacke et al., 2005)). Because the sustained hepatic inflammation induced by various etiologies leads to liver fibrosis, and NF-κB plays a critical role in regulating

inflammatory responses (Luedde and Schwabe, 2011), we tried to apply NF-κB transgenic mice to report the liver fibrosis induced by CCl_4. CCl_4 induced the NF-κB-dependent luminescence in the liver with specificity and the NF-κB activation was correlated with liver fibrosis, judged by Sirius red staining and immunohistochemical analysis. These findings indicated the feasibility of NF-κB bioluminescent imaging on the reporting of liver fibrosis induced by CCl_4.

Silymarin is a well-known hepatoprotective agent for the treatment of liver diseases (Abenavoli et al., 2010). It possesses antioxidative, antilipid peroxidative, antifibrotic, membrane stabilizing, immunomodulatory, and liver regenerating activities (Polyak et al., 2007; Saller et al., 2001; Shaker et al., 2010). Silymarin offers a good protection in various models of experimental liver diseases. It has also been applied clinically for alcoholic liver diseases, liver cirrhosis, Amanita mushroom poisoning, and drug-induced liver diseases (Pradhan and Girish, 2006). In this study, bioluminescent imaging showed that oral administration of silymarin reduced the CCl_4-induced NF-κB-dependent luminescent intensity in the liver with specificity. The correlation of the decreased NF-κB activity and the improved liver fibrosis by silymarin, suggesting the feasibility of NF-κB-dependent bioluminescent imaging for the evaluation of therapeutic effect of silymarin *in vivo*.

NF-κB bioluminescent imaging-guided transcriptomic analysis was further applied for the evaluation of novel targets and mechanisms of silymarin-mediated protection in the liver. Previous studies indicated that the anti-fibrotic and anti-inflammatory effects of silymarin are associated with TGF-β1 pathway (Ai et al., 2010). Silymarin suppresses the expression of profibrotic procollagen-α and TIMP-1 via downregulation of TGF-β1 mRNA in rats with biliary fibrosis (Jia et al., 2001). Moreover, genes associated with oxidative stress, cell cycle, cytoskeletal network,

cell-cell adhesion, extracellular matrix, inflammation, and apoptosis are altered by silymarin in pyrogallol-exposed liver (Upadhyay et al., 2010). In this study, microarray data showed that silymarin altered the TGF-β1-associated pathways, including TGF-β signaling pathway, TGF-β-induced apoptosis and TGF-β-mediated pathway, in CCl_4-induced liver fibrosis, which were in agreement with previous reports. Furthermore, we newly identified that silymarin downregulated the expression levels of cytoskeleton organization genes and mitochondrion electron-transfer chain genes. It has been known that CCl_4 treatment induces the reorganization of cytoskeleton and, in turn, induces the differentiation of hepatic stellate cells into myofibroblast-like cells ((De Minicis et al., 2007). Silymarin downregulated the expression of cytoskeleton component genes, suggesting that silymarin might suppress the transformation of hepatic stellate cells via inhibiting cytoskeleton reorganization and thus ameliorate the fibrosis of liver. Progression of CCl_4-induced liver fibrosis is associated with free radicals production that results in the significant alternations in functional state of mitochondrial respiratory chain (Tanaka et al., 1987). The electron transporters are combined in four complex: NADH reductase, succinate reductase, cytochrome *c* reductase, and Cox (Boyer, 1997). Cox plays a crucial role in oxidative metabolism, acting as the terminal component of the mitochondrial electron-transport chain in which electrons are passed from cytochrome *c* to molecular oxygen (Boyer, 1997). Previous studies showed that CCl_4 treatment decreases the activity of NADH reductase and increases the activity of Cox in rats with CCl_4-induced liver fibrosis (Krahenbuhl and Reichen, 1992; Shiryaeva et al., 2008; Tanaka et al., 1987). Our data also showed that the expression levels of Cox genes were elevated by CCl_4. The decrease and damage of NADH reductase results in electron leakage to $\cdot O_2^-$ oxygen and superoxide anion production, which lead to the

increased oxygen consumption by the respiratory chain of pathologic mitochondria. Subsequently, the elevated activity of Cox by CCl_4 promotes the transfer of electrons to molecular oxygen and drive the ATP production of the mitochondria (Shiryaeva et al., 2008). In contrast, previous study indicated that silymarin inhibits the oxygen consumption in mitochondria isolated from rats and increases the iron-reduced NADH reductase activity to the basal level (Chavez and Bravo, 1988; Pietrangelo et al., 2002). Moreover, our data showed that silymarin reduced the CCl_4-induced expression levels of Cox genes to the basal levels as compared to mock. These findings suggested that silymarin might counteract the mitochondrion electron-transfer chain alteration by CCl_4, which might be associated with the improvement of CCl_4-induced liver fibrosis by silymarin.

5. Conclusions

In conclusion, we applied for the first time the *in vivo* NF-κB bioluminescent imaging and microarray analysis for the evaluation and identification of the therapeutic potentials and novel mechanisms of silymarin in CCl_4-induced liver fibrosis. The correlation of NF-κB bioluminescence and liver fibrosis suggested the feasibility of NF-κB bioluminescent imaging on the evaluation of therapeutic potentials of drugs for the treatment of liver fibrosis. Moreover, we newly identified that silymarin exhibited anti-fibrotic effects *in vivo* via regulating TGF-β-mediated pathways and altering the expression of genes involved in cytoskeleton organization and mitochondrion electron-transfer chain.

Conflict of Interest

The authors declare that there are no conflicts of interest.

Acknowledgments

This work was supported by grants from National Science Council, Committee on Chinese Medicine and Pharmacy at Department of Health (CCMP100-RD-048), and China Medical University (CMU100-S-16, CMU100-S-34, and CMU100-TS-14).

References

Abenavoli, L., Capasso, R., Milic, N., Capasso, F., 2010. Milk thistle in liver diseases: past, present, future. Phytother Res 24, 1423-1432.

Ai, W., Zhang, Y., Tang, Q.Z., Yan, L., Bian, Z.Y., Liu, C., Huang, H., Bai, X., Yin, L., Li, H., 2010. Silibinin attenuates cardiac hypertrophy and fibrosis through blocking EGFR-dependent signaling. J Cell Biochem 110, 1111-1122.

Baeuerle, P.A., Baichwal, V.R., 1997. NF-κB as a frequent target for immunosuppressive and anti-inflammatory molecules. Adv Immunol. 65, 111-137.

Baldwin, A.S., Jr., 1996. The NF-κB and IκB proteins: new discoveries and insights. Annu Rev Immunol 14, 649-683.

Basiglio, C.L., Sanchez Pozzi, E.J., Mottino, A.D., Roma, M.G., 2009. Differential effects of silymarin and its active component silibinin on plasma membrane stability and hepatocellular lysis. Chem Biol Interact 179, 297-303.

Bataller, R., Brenner, D.A., 2005. Liver fibrosis. J Clin Invest 115, 209-218.

Baur, J.A., Pearson, K.J., Price, N.L., Jamieson, H.A., Lerin, C., Kalra, A., Prabhu, V.V., Allard, J.S., Lopez-Lluch, G., Lewis, K., Pistell, P.J., Poosala, S., Becker, K.G., Boss, O., Gwinn, D., Wang, M., Ramaswamy, S., Fishbein, K.W., Spencer, R.G., Lakatta, E.G., Le Couteur, D., Shaw, R.J., Navas, P., Puigserver, P., Ingram, D.K., de Cabo, R., Sinclair, D.A., 2006. Resveratrol improves health and survival of mice on a high-calorie diet. Nature 444, 337-342.

Bonizzi, G., Karin, M., 2004. The two NF-κB activation pathways and their role in innate and adaptive immunity. Trends Immunol 25, 280-288.

Boyer, P.D., 1997. The ATP synthase--a splendid molecular machine. Annual review of biochemistry 66, 717-749.

Chandan, B.K., Saxena, A.K., Shukla, S., Sharma, N., Gupta, D.K., Singh, K., Suri, J., Bhadauria, M., Qazi, G.N., 2008. Hepatoprotective activity of Woodfordia fruticosa Kurz flowers against carbon tetrachloride induced hepatotoxicity. J Ethnopharmacol 119, 218-224.

Chang, C.T., Lin, H., Ho, T.Y., Li, C.C., Lo, H.Y., Wu, S.L., Huang, Y.F., Liang, J.A., Hsiang, C.Y., 2011. Comprehensive assessment of host responses to ionizing radiation by nuclear factor-κB bioluminescence imaging-guided transcriptomic analysis. PLoS ONE, in press.

Chavez, E., Bravo, C., 1988. Silymarin-induced mitochondrial Ca2+ release. Life Sci 43, 975-981.

Cheng, H.M., Li, C.C., Chen, C.Y., Lo, H.Y., Cheng, W.Y., Lee, C.H., Yang, S.Z., Wu, S.L., Hsiang, C.Y., Ho, T.Y., 2010. Application of bioactivity database of Chinese herbal medicine on the therapeutic prediction, drug development, and safety evaluation. J Ethnopharmacol 132, 429-437.

Comporti, M., Arezzini, B., Signorini, C., Vecchio, D., Gardi, C., 2009. Oxidative stress, isoprostanes and hepatic fibrosis. Histol Histopathol 24, 893-900.

Contag, C.H., Bachmann, M.H., 2002. Advances in *in vivo* bioluminescence imaging of gene expression. Annu Rev Biomed Eng 4, 235-260.

De Minicis, S., Seki, E., Uchinami, H., Kluwe, J., Zhang, Y., Brenner, D.A., Schwabe, R.F., 2007. Gene expression profiles during hepatic stellate cell activation in culture and *in vivo*. Gastroenterology 132, 1937-1946.

Dothager, R.S., Flentie, K., Moss, B., Pan, M.H., Kesarwala, A., Piwnica-Worms, D., 2009. Advances in bioluminescence imaging of live animal models. Curr Opin Biotechnol 20, 45-53.

Hellerbrand, C., Stefanovic, B., Giordano, F., Burchardt, E.R., Brenner, D.A. 1999.

The role of TGFβ1 in initiating hepatic stellate cell activation *in vivo*. J Hepatol 30, 77-87.

Ho, T.Y., Chen, Y.S., Hsiang, C.Y., 2007. Noninvasive nuclear factor-κB bioluminescence imaging for the assessment of host-biomaterial interaction in transgenic mice. Biomaterials 28, 4370-4377.

Hseu, Y.C., Huang, H.C., Hsiang, C.Y., 2010. *Antrodia camphorata* suppresses lipopolysaccharide-induced nuclear factor-κB activation in transgenic mice evaluated by bioluminescence imaging. Food Chem Toxicol 48, 2319-2325.

Hsiang, C.Y., Chen, Y.S., Ho, T.Y., 2009. Nuclear factor-κB bioluminescence imaging-guided transcriptomic analysis for the assessment of host-biomaterial interaction *in vivo*. Biomaterials 30, 3042-3049.

Jia, J.D., Bauer, M., Cho, J.J., Ruehl, M., Milani, S., Boigk, G., Riecken, E.O., Schuppan, D., 2001. Antifibrotic effect of silymarin in rat secondary biliary fibrosis is mediated by downregulation of procollagen alpha1(I) and TIMP-1. J Hepatol 35, 392-398.

Jimenez, W., Pares, A., Caballeria, J., Heredia, D., Bruguera, M., Torres, M., Rojkind, M., Rodes, J., 1985. Measurement of fibrosis in needle liver biopsies: evaluation of a colorimetric method. Hepatology 5, 815-818.

Karin, M., Ben-Neriah, Y., 2000. Phosphorylation meets ubiquitination: the control of NF-κB activity. Annu Rev Immunol 18, 621-663.

Krahenbuhl, S., Reichen, J., 1992. Adaptation of mitochondrial metabolism in liver cirrhosis. Different strategies to maintain a vital function. Scand J Gastroenterol Suppl 193, 90-96.

Lamb, J., Crawford, E.D., Peck, D., Modell, J.W., Blat, I.C., Wrobel, M.J., Lerner, J., Brunet, J.P., Subramanian, A., Ross, K.N., Reich, M., Hieronymus, H., Wei, G.,

Armstrong, S.A., Haggarty, S.J., Clemons, P.A., Wei, R., Carr, S.A., Lander, E.S., Golub, T.R., 2006. The Connectivity Map: using gene-expression signatures to connect small molecules, genes, and disease. Science 313, 1929-1935.

Lopez-De Leon, A., Rojkind, M., 1985. A simple micromethod for collagen and total protein determination in formalin-fixed paraffin-embedded sections. J Histochem Cytochem 33, 737-743.

Lotersztajn, S., Julien, B., Teixeira-Clerc, F., Grenard, P., Mallat, A., 2005. Hepatic fibrosis: molecular mechanisms and drug targets. Annu Rev Pharmacol Toxicol 45, 605-628.

Luedde, T., Schwabe, R.F., 2011. NF-κB in the liver--linking injury, fibrosis and hepatocellular carcinoma. Nat Rev Gastroenterol Hepatol 8, 108-118.

Nanji, A.A., Jokelainen, K., Tipoe, G.L., Rahemtulla, A., Dannenberg, A.J., 2001. Dietary saturated fatty acids reverse inflammatory and fibrotic changes in rat liver despite continued ethanol administration. J Pharmacol Exp Ther 299, 638-644.

Ottobrini, L., Lucignani, G., Clerici, M., Rescigno, M., 2005. Assessing cell trafficking by noninvasive imaging techniques: applications in experimental tumor immunology. Q J Nucl Med Mol Imaging 49, 361-366.

Pietrangelo, A., Montosi, G., Garuti, C., Contri, M., Giovannini, F., Ceccarelli, D., Masini, A., 2002. Iron-induced oxidant stress in nonparenchymal liver cells: mitochondrial derangement and fibrosis in acutely iron-dosed gerbils and its prevention by silybin. J Bioenerg Biomembr 34, 67-79.

Polyak, S.J., Morishima, C., Shuhart, M.C., Wang, C.C., Liu, Y., Lee, D.Y., 2007. Inhibition of T-cell inflammatory cytokines, hepatocyte NF-κB signaling, and HCV infection by standardized Silymarin. Gastroenterology 132, 1925-1936.

Pradhan, S.C., Girish, C., 2006. Hepatoprotective herbal drug, silymarin from

experimental pharmacology to clinical medicine. Indian J Med Res 124, 491-504.

Sakaida, I., Terai, S., Yamamoto, N., Aoyama, K., Ishikawa, T., Nishina, H., Okita, K., 2004. Transplantation of bone marrow cells reduces CCl_4-induced liver fibrosis in mice. Hepatology 40, 1304-1311.

Saller, R., Meier, R., Brignoli, R., 2001. The use of silymarin in the treatment of liver diseases. Drugs 61, 2035-2063.

Sarraf-Yazdi, S., Mi, J., Dewhirst, M.W., Clary, B.M., 2004. Use of *in vivo* bioluminescence imaging to predict hepatic tumor burden in mice. J Surg Res 120, 249-255.

Shaker, E., Mahmoud, H., Mnaa, S., Silymarin, the antioxidant component and *Silybum marianum* extracts prevent liver damage. Food Chem Toxicol 48, 803-806.

Shiryaeva, A., Baidyuk, E., Arkadieva, A., Okovityy, S., Morozov, V., Sakuta, G., 2008. Hepatocyte mitochondrion electron-transport chain alterations in CCl_4 and alcohol induced hepatitis in rats and their correction with simvastatin. J Bioenerg Biomembr 40, 27-34.

Siebenlist, U., Franzoso, G., Brown, K., 1994. Structure, regulation and function of NF-κB. Annu Rev Cell Biol 10, 405-455.

Sun, H., Che, Q.M., Zhao, X., Pu, X.P., 2010. Antifibrotic effects of chronic baicalein administration in a CCl_4 liver fibrosis model in rats. Eur J Pharmacol 631, 53-60.

Suter, L., Babiss, L.E., Wheeldon, E.B., 2004. Toxicogenomics in predictive toxicology in drug development. Chem Biol 11, 161-171.

Tacke, F., Wustefeld, T., Horn, R., Luedde, T., Srinivas Rao, A., Manns, M.P., Trautwein, C., Brabant, G., 2005. High adiponectin in chronic liver disease and cholestasis suggests biliary route of adiponectin excretion *in vivo*. J Hepatol 42,

666-673.

Tanaka, A., Morimoto, T., Wakashiro, S., Ikai, I., Ozawa, K., Orii, Y., 1987. Kinetic alterations of cytochrome *c* oxidase in carbon tetrachloride induced cirrhotic rat liver. Life Sci 41, 741-748.

Upadhyay, G., Tiwari, M.N., Prakash, O., Jyoti, A., Shanker, R., Singh, M.P., 2010. Involvement of multiple molecular events in pyrogallol-induced hepatotoxicity and silymarin-mediated protection: evidence from gene expression profiles. Food Chem Toxicol 48, 1660-1670.

Weiler-Normann, C., Herkel, J., Lohse, A.W., 2007. Mouse models of liver fibrosis. Z Gastroenterol 45, 43-50.

Wells, R.G., 2005. The role of matrix stiffness in hepatic stellate cell activation and liver fibrosis. J Clin Gastroenterol 39, S158-161.

Wu, S.L., Chen, J.C., Li, C.C., Lo, H.Y., Ho, T.Y., Hsiang, C.Y., 2009. Vanillin improves and prevents trinitrobenzene sulfonic acid-induced colitis in mice. J Pharmacol Exp Ther 330, 370-376.

Xiong, Y.Q., Willard, J., Kadurugamuwa, J.L., Yu, J., Francis, K.P., Bayer, A.S., 2005. Real-time *in vivo* bioluminescent imaging for evaluating the efficacy of antibiotics in a rat Staphylococcus aureus endocarditis model. Antimicrob Agents Chemother 49, 380-387.

Figure captions

Fig. 1. NF-κB-dependent bioluminescence in living mice. Transgenic mice were administered with CCl_4 and/or silymarin, and imaged at indicated periods. (A) *In vivo* imaging. The color overlay on the image represents the photon/sec emitted from the animal, as indicated by the color scales. Photos are representative images (n=8). (B) Quantification of photon emission from whole animal. Values are mean ± standard error (n=8). ###p<0.001, compared with mock. *p<0.05, **p<0.01, compared with CCl_4.

Fig. 2. NF-κB-dependent bioluminescence in individual organs. Transgenic mice were administered with CCl_4 and/or silymarin. Twelve weeks later, mice were sacrificed and organs were subjected to image. (A) *Ex vivo* imaging. The color overlay on the image represents the photon/sec emitted from the organ, as indicated by the color scales. Photos are representative images (n=8). (B) Quantification of photon emission from organs. Values are mean ± standard error (n=8). ###p<0.001, compared with mock. ***p<0.001, compared with CCl_4.

Fig. 3. Histological examination of liver by H&E and Sirius red staining. (A) Histological examination. Transgenic mice were administered with CCl_4 and/or silymarin. Twelve weeks later, mice were sacrificed, livers were excised, and sections were stained with H&E (100× magnification) or Sirius red (40× magnification). Photos are representative images (n=8). (B) Quantification of liver fibrosis by Sirius red stain. Results are expressed as fibrotic area (%), which was calculated as areas occupied with red color/area of whole tissue. Values are mean ± standard error (8 sections/group and 10 fields/section). ###p<0.001, compared with

mock. ***p<0.001, compared with CCl_4.

Fig. 4. Immunohistochemical examination of liver. Transgenic mice were administered with CCl_4 and/or silymarin. Twelve weeks later, mice were sacrificed, livers were excised, and sections were immunostained with antibodies against TGF-β1, α-SMA, and p65 (100× magnification). Quantification of TGF-β1, α-SMA, and p65-positive areas (%) was shown at the bottom. Values are mean ± standard error (8 sections/group and 3 fields/section). Photos are representative images (n=8).

Table1

Pathway analysis of silymarin-altered genes with fold changes ≥2.0 or ≤–2.0.

Pathway	*p* value[a]
Regulation of cellular process/ cell cycle and death	
TGF-β signaling pathway	2.75×10^{-7}
p53-mediated pathway	0.00171
Tight junction	0.00014
TGF-β-induced apoptosis	0.00261
Adherens junction	0.00494
TGF-β-mediated pathway	0.00976
Metabolism	
Urea cycle and metabolism of amino groups	2.49×10^{-5}
Citrate cycle	2.45×10^{-6}
Arginine and proline metabolism	0.00016
Galactose metabolism	0.00034
Biosynthesis of steroids	0.00049
Glycine, serine and threonine metabolism	0.00070
Glycolysis / Gluconeogenesis	0.00100
Butanoate metabolism	0.00098
Folate biosynthesis	0.00218
Pyruvate metabolism	0.00223
Fatty acid metabolism	0.00273
Bile acid biosynthesis	0.00273
Alanine and aspartate metabolism	0.00442
Glutathione metabolism	0.00544
Starch and sucrose metabolism	0.00601
Glycosaminoglycan degradation	0.00799
Glutamate metabolism	0.00921
Signal tansduction	
Adipocytokine signaling pathway	8.26×10^{-5}
IL6 signaling pathway	0.00016
PPAR signaling pathway	0.00039
Insulin signaling pathway	0.00047
Vitamin D3 signaling pathway	0.00067
RANKL signaling pathway	0.00548
TNF signaling pathway	0.00629
IGF signaling pathway	0.00655
Chemokine signaling pathway	0.00709
EGF signaling pathway	0.00770
PTH/PTHrP signaling pathway	0.00840

[a] *p* value was calculated on WebGestalt web site by hypergeometric test.

Table 2

Expression levels of silymarin-downregulated genes in CCl_4-treated liver.

Gene symbol	Description	Fold changes[a]
Acta1	Actin, alpha 1, skeletal muscle	-90.21±0.001
Myl1	Myosin, light polypeptide 1	-77.05±0.001
Tnni2	Troponin I, skeletal, fast 2	-49.39±0.001
Atp2a1	ATPase, Ca^{+2} transporting, cardiac muscle, fast twitch 1	-48.46±0.001
Mylpf	Myosin light chain, phosphorylatable, fast skeletal muscle	-41.90±0.001
Mb	Myoglobin	-35.39±0.002
Cox6a2	Cytochrome c oxidase, subunit VI a, polypeptide 2	-28.43±0.003
Cox8b	Cytochrome c oxidase, subunit VIII b	-18.60±0.004
Eno3	Enolase 3, beta muscle	-8.17±0.009
Tnnt1	Troponin T1, skeletal, slow	-7.60±0.011
Tnnc1	Troponin C, cardiac/slow skeletal	-7.56±0.010
Cox7a1	Cytochrome c oxidase, subunit VIIa 1	-6.67±0.015
Eef1a2	Eukaryotic translation elongation factor 1 alpha 2	-4.64±0.022
EG433229	Predicted gene, EG433229, transcript variant 7	-4.06±0.016

[a] Fold changes are mean ± standard error (n=3).

Table 3

Expression levels of Cox6a2, Cox7a1, and Cox8b genes by qPCR.

Sample	Average C_T of target	Average C_T of GAPDH	ΔC_T[a]	$\Delta\Delta C_T$[b]	Relative to mock
Cox6a2					
Mock	35.82 ± 0.40	19.71 ± 0.03	16.11 ± 0.40	0.00 ± 0.40	1.00
CCl_4	25.80 ± 0.05	18.64 ± 0.05	7.16 ± 0.07	-8.96 ± 0.07	496.21
Silymarin	31.17 ± 0.09	18.36 ± 0.01	12.81 ± 0.09	-3.30 ± 0.09	9.84
Cox7a1					
Mock	29.98 ± 0.10	19.71 ± 0.03	10.27 ± 0.11	0.00 ± 0.11	1.00
CCl_4	24.49 ± 0.04	18.64 ± 0.05	5.85 ± 0.07	-4.42 ± 0.07	21.36
Silymarin	29.10 ±0 .11	18.36 ± 0.01	10.74 ± 0.11	0.47 ± 0.11	0.72
Cox8b					
Mock	32.81 ± 0.11	19.71 ± 0.03	13.09 ± 0.12	0.00 ± 0.12	1.00
CCl_4	23.83 ± 0.05	18.64 ± 0.05	5.18 ± 0.07	-7.91 ± 0.07	240.38
Silymarin	31.97 ± 0.29	18.36 ± 0.01	13.61 ± 0.29	0.52 ± 0.29	0.70

[a] The ΔC_T value is determined by subtracting the average GAPDH C_T value from the average target gene C_T value. The standard deviation of the difference is calculated from the standard deviations of the target gene and GAPDH.

[b] The calculation of $\Delta\Delta C_T$ involves subtraction by the ΔC_T calibrator value. This is a subtraction of an arbitrary constant, so the standard

deviation of$\Delta\Delta C_T$ is the same as the standard deviation of ΔC_T value.

Figure 1

Click here to download high resolution image

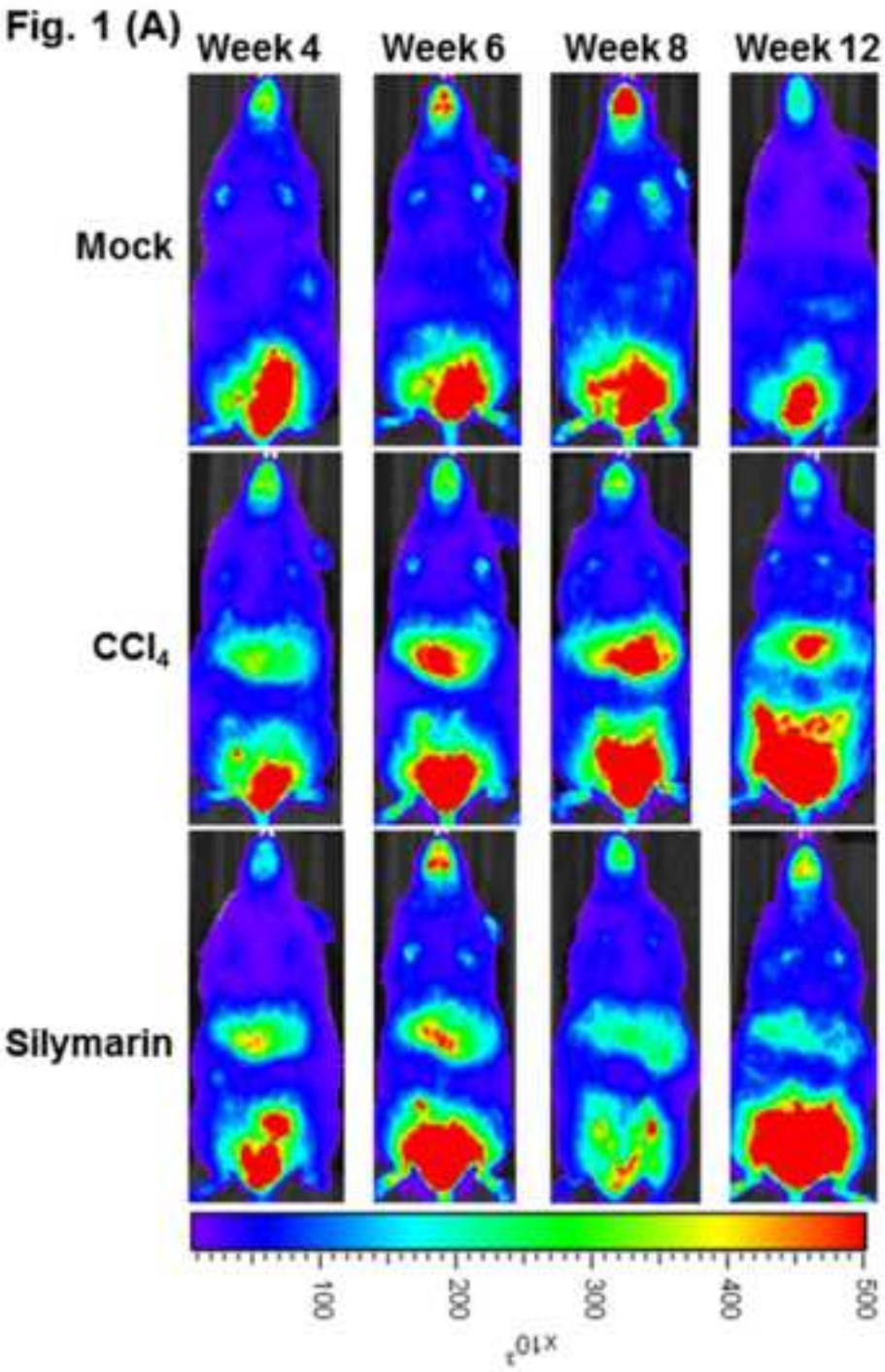

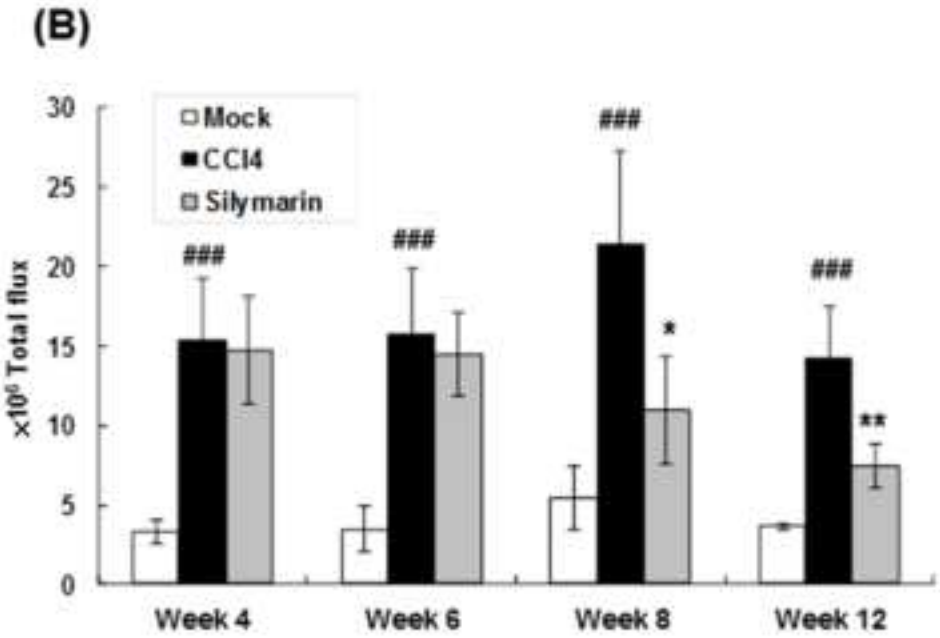

Figure 2

Click here to download high resolution image

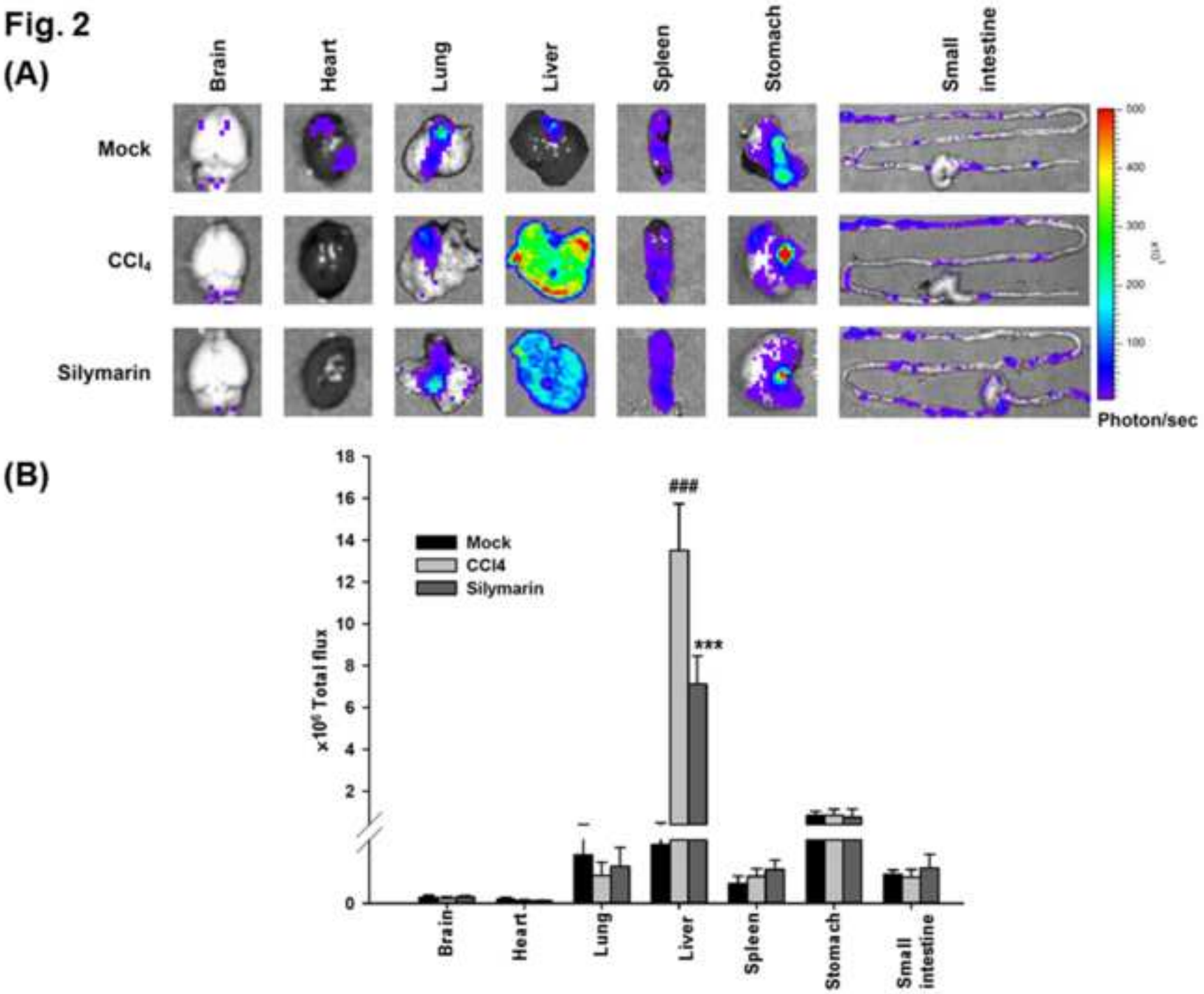

Figure 3
Click here to download high resolution image

Fig. 3

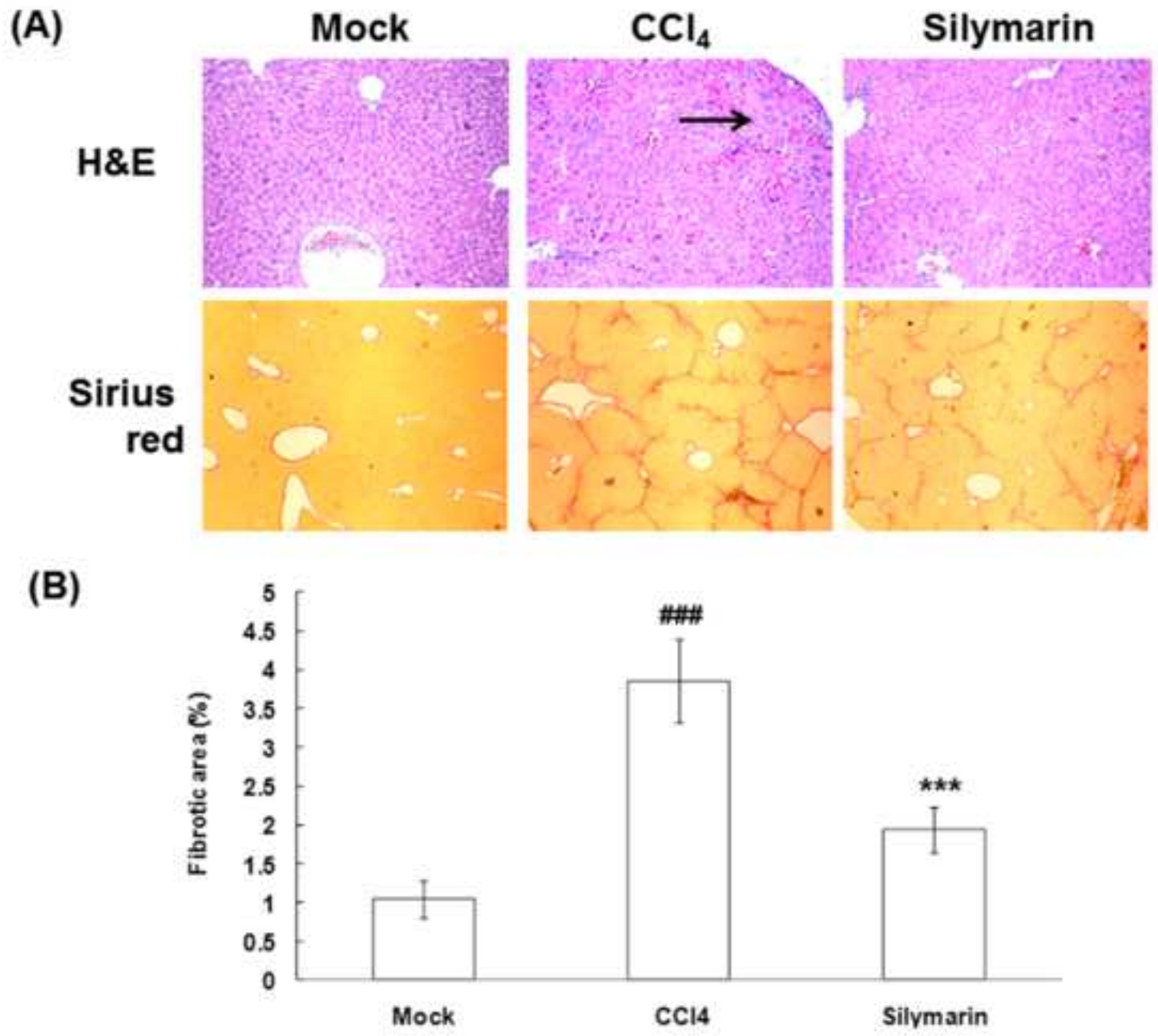

Figure 4

Click here to download high resolution image

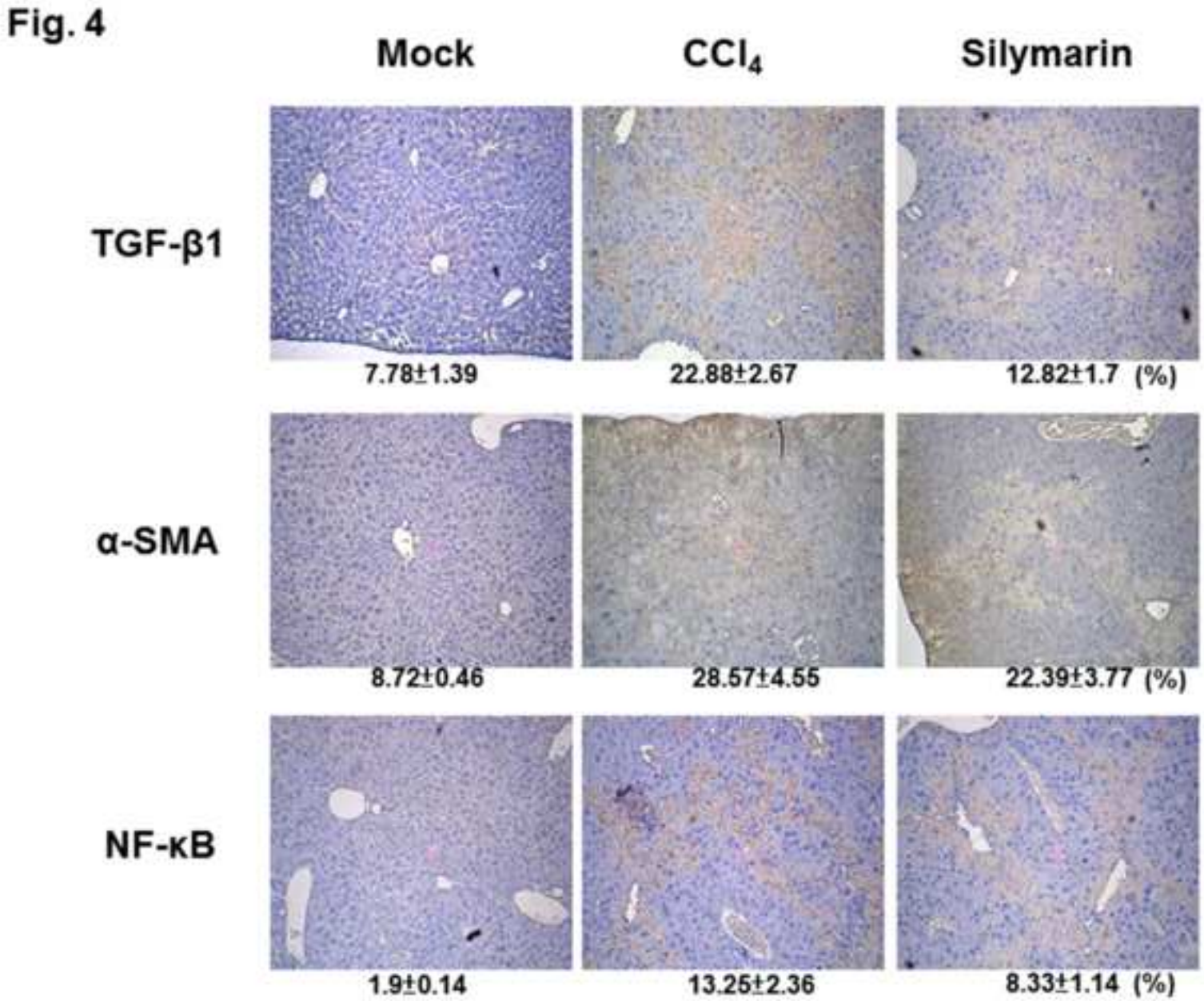

Abstract

In this study, we applied bioluminescent imaging-guided transcriptomic analysis to evaluate and identify the therapeutic potentials and novel mechanisms of silymarin on carbon tetrachloride (CCl_4)-induced liver fibrosis. Transgenic mice, carrying the luciferase genes driven by nuclear factor-κB (NF-κB), were given with CCl_4 and/or silymarin. *In vivo* NF-κB activity was evaluated by bioluminescent imaging, liver fibrosis was judged by Sirius red staining and immunohistochemistry, and gene expression profiles of silymarin-treated livers were analyzed by DNA microarray. CCl_4 enhanced the NF-κB-dependent hepatic luminescence and induced hepatic fibrosis, while silymarin reduced the CCl_4-induced hepatic luminescence and improved CCl_4-induced liver fibrosis. Microarray analysis showed that silymarin altered the transforming growth factor-β-mediated pathways, which play pivotal roles in the progression of liver fibrosis. Moreover, we newly identified that silymarin downregulated the expression levels of cytoskeleton organization genes and mitochondrion electron-transfer chain genes, such as cytochrome *c* oxidase Cox6a2, Cox7a1, and Cox8b genes. In conclusion, the correlation of NF-κB-dependent luminescence and liver fibrosis suggested the feasibility of NF-κB bioluminescent imaging for the evaluation of liver fibrosis progression and therapeutic potentials. Moreover, our findings suggested that silymarin might exhibit anti-fibrotic effects *in vivo* via altering the expression of genes involved in cytoskeleton organization and mitochondrion electron-transfer chain.

Keywords: Liver fibrosis, Silymarin, Nuclear factor-κB, Bioluminescent imaging, DNA microarray, Cytochrome *c* oxidase